NASA/TP-2000-210083
AMCOM-AFDD/TR-00-A-007

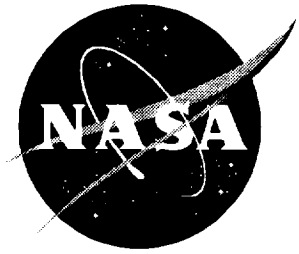

Exploratory Investigation of Aerodynamic Characteristics of Helicopter Tail Boom Cross-Section Models With Passive Venting

Daniel W. Banks
Dryden Flight Research Center, Edwards, California

Henry L. Kelley
U.S. Army Aviation and Missile Command (AMCOM)
Aeroflightdynamics Directorate
Joint Research Program Office
NASA Langley Research Center, Hampton, Virginia

National Aeronautics and
Space Administration

Langley Research Center
Hampton, Virginia 23681-2199

June 2000

Available from:

NASA Center for AeroSpace Information (CASI)
7121 Standard Drive
Hanover, MD 21076-1320
(301) 621-0390

National Technical Information Service (NTIS)
5285 Port Royal Road
Springfield, VA 22161-2171
(703) 605-6000

Summary

An exploratory wind-tunnel investigation was conducted to determine the effectiveness of passively venting two representative models of helicopter tail boom shapes to reduce side force and down load during simulated hover and sideward flight conditions. A two-dimensional tail boom model with two different cross-sectional shapes was used. One shape was oval, representative of a UH-60 (medium size, single main rotor helicopter with a tail rotor) tail boom, and the other was a trapezoidal cross section, representative of a potential low-observable shape. The models were 1/2-scale cross sections (relative to the full-scale UH-60 helicopter tail boom) of the location at the mid to aft part of the boom approximately located at the position under the 80-percent rotor radius. Various venting schemes were investigated with a porous skin covering the models. Completely porous and completely solid configurations were tested, as well as configurations which simulated partial venting in various symmetric and asymmetric cases. Selected venting schemes were also investigated in conjunction with single and double tail boom strakes. Calculations of engine power required were made by using model coefficients to evaluate effects of the various configurations on power required from the main rotor and tail rotor of a full-size helicopter. These results are then compared with the calculated results obtained from the fully solid oval and the fully solid trapezoidal boom.

The results indicate that passively venting a helicopter tail boom can alleviate some of the adverse side forces that are generated in hover and sideward flight and reduce the overall power required. A penalty of increased down load is attributed to the increased skin friction as a result of the porous surface. This down load penalty can be reduced or eliminated by properly sizing hole parameters. In addition, the side force behavior as a function of incidence angle of the vented configurations was smoother and exhibited a less abrupt boom stall than indicated by the baseline configuration. The smoother characteristics of the vented configurations may result in fewer yaw control disturbances during flight in gusty air conditions.

Introduction

The tail boom of a single rotor helicopter is subjected to a complex flow field generated by the main and tail rotor wakes, the free-stream flow, and the wake from the forward fuselage. Hover and sideward flight present the most critical flight regimes in terms of adverse side and down loads on the tail boom. To overcome this adverse loading, additional engine power is required in many flight conditions. The two conditions reduce payload, performance, and available yaw control margins. Nonlinear force gradients near conditions of boom stall can also make precision yaw control more difficult for the pilot. In practice, a good tail boom design, from an aerodynamics standpoint, should minimize the down load and the adverse fuselage yawing moments. Some tail boom designs actively control the circulation around them to minimize adverse forces (the no tail rotor configuration or NOTAR, ref. 1), which must be driven, in part, from engine power. Other designs attempt to disrupt the adverse circulation about the boom by using strakes or spoilers (refs. 2, 3, and 4).

In recent research for fixed-wing aircraft, the application of a porous surface has been used to alter surface pressure distribution (refs. 5 and 6). It was postulated that, by passively venting portions of a helicopter tail boom (generally representative of a blunt body shape), the pressure distribution and, therefore, the loading on the boom could be modified in a favorable way. Various venting schemes are suggested as possibilities for future investigations, and they could potentially be used in conjunction with other methods, such as tail boom strakes or NOTAR. These methods include, but are not limited to, the use of porous material on all or parts of the boom opening to a specific plenum or the boom cavity, and the use of doors, grilles, slots, or other openings. Furthermore, it may be useful to capture a portion of the relatively high velocity downwash from the main rotor as it impacts the upper surface of the boom and channel that flow to another area on the boom.

In an effort to obtain some preliminary results from this concept, an exploratory wind-tunnel investigation was conducted to determine whether passively venting the boom could modify the pressure loading such that the adverse forces and moments could be reduced. This study was conducted in the Langley 14- by 22-Foot Subsonic Tunnel with two 1/2-scale two-dimensional tail boom shapes. The shapes were representative of the tail booms from a UH-60 (oval cross section) and of a low-observable design

(trapezoidal cross section) both with the tail rotor drive shaft cover (TRDSC) on. The UH-60 helicopter is shown in figure 1. The normal and side forces were measured at free-stream dynamic pressures up to 30 psf, which include full-scale Reynolds numbers, and incidence angles from −90° to +90° to simulate left and right crosswinds. Calculations were made by using the normal and side force coefficients to determine the trends of the aerodynamic forces on the boom of a full-scale UH-60 helicopter, and the estimated main rotor power and the tail rotor power required to trim those forces were compared with the solid baseline oval and trapezoidal shapes. A summary of the findings of this exploratory investigation is presented herein.

Symbols

All force and moment data have been reduced to coefficient form. The positive sense of the model incidence and aerodynamic coefficients is given in figure 2(b).

b maximum width of model normal to flow at zero incidence angle, ft (see fig. 2(b))

c maximum depth of model parallel to flow at zero incidence angle, ft (see fig. 2(b))

c_y section side force coefficient, $\dfrac{\text{Side force per unit length}}{bq_\infty}$

c_z section normal force coefficient, $\dfrac{\text{Normal force per unit length}}{bq_\infty}$

HP_{DL} calculated power required for main rotor to trim tail boom normal force, positive value indicates boom had upward force, hp

HP_{net} sum of HP_{DL} and HP_{SL}; that is, total calculated power required to trim aerodynamic forces on tail boom, hp

HP_{saved} HP_{net} of given configuration minus HP_{net} of solid baseline, hp

HP_{SL} calculated power required of tail rotor to trim tail boom side force, positive value indicates boom had side force to starboard side, hp

N_B boom down load, $c_z qS$, lbf

q estimated local dynamic pressure under main rotor at top of tail boom during hover and crosswind flight, psf

q_∞ free-stream dynamic pressure in tunnel, $\frac{1}{2}\rho V_\infty^2$, psf

r radius, in.

Re Reynolds number, $\dfrac{\rho V_\infty c}{\mu}$

S reference area (vertically projected) for tail boom shapes, $b \times$ length, ft^2

TRDSC tail rotor drive shaft cover

V_∞ free-stream velocity in tunnel, ft/sec

Y_B boom side force, $c_y qS$, lbf

Y_T tail rotor thrust, lbf

μ absolute viscosity, slug/ft-sec

ρ free-stream air density, slug/ft^3

ϕ angle of flow incidence in plane normal to axis of two-dimensional cylinder, deg (see fig. 2(b))

Models and Apparatus

Two 1/2-scale, two-dimensional models representative of helicopter tail boom cross sections were tested. Sketches and photographs of the models and test apparatus are shown in figures 2 and 3. One model, oval in cross section, was representative of a UH-60 helicopter tail boom (fig. 2(c)) and the other model with a trapezoidal cross section was representative of an advanced low-observable configuration boom (fig. 2(d)). Each model also had a simulated tail rotor drive shaft cover (TRDSC) on the top. The models were constructed of aluminum bulkheads with the

skins made of porous stainless steel sheets with flush-mounted screws. The porous skins were 0.018 in. thick with 0.030-in-diameter holes located on 0.063-in. centers (equivalent to 18 percent porosity). The hole size, spacing, and thickness of the porous material were not optimum (ref. 5); however, the material was the closest that was commercially available. An optimum material would have sufficient porosity to allow rapid pressure equalization, with holes small enough not to cause premature transition or increased surface friction from the apparent roughness (a ratio of skin thickness to hole diameter greater than 2 has been shown to minimize skin friction, ref. 5). This commercially available porous material, though not optimum, was thought to be suitable to obtain preliminary data in the investigation of the effectiveness of using this scheme to reduce the adverse forces experienced by the tail boom.

The model consisted of three external sections—two rigidly mounted nonmetric sections at the top and bottom with solid surfaces and the metric test section in the middle with porous surfaces. (See fig. 3(a).) End plates were mounted at the end of the two rigidly mounted sections to minimize spanwise flow. The metric test section (middle 40 in.) was attached to a six-component strain-gauge balance (fig. 3(c)), although only the normal force and side force components were of interest and analyzed.

To simulate both the amount of venting and the locations of the vents, a portion of the porous model was covered with wide plastic tape. An example of the taping is shown in figure 4. To ensure that this taping had no effect on the general characteristics of the model, the entire metric model section was taped over and the wind tunnel test procedure was verified by comparison with previous data with a solid-skinned model (ref. 2). Strakes were also tested with various venting configurations. Strakes were either 1.5 or 2 in. in height and 1/8 in. thick. (See fig. 5.) The various venting schemes progressed from fully porous to fully solid as shown in figure 5. Intermediate configurations included porous booms with solid (taped) TRDSC, porous boom sides with solid bottom and top (including TRDSC), and 1/2 and 1/4 porous sides with the rest solid. In addition to the symmetric configurations, there were two asymmetric configurations where the porous areas were not symmetric from side to side. The asymmetric configurations were tested only on the oval boom. The low asymmetric configuration (O6) (fig. 5(a)) consisted of a partially porous side (9.25 in.) and a porous corner (6 in.) on the opposite side. The high asymmetric configuration (O7) consisted of a porous side (9.25 in.) and a porous upper corner (5 in.) on the opposite side. The asymmetric configurations were investigated to determine if the pressure distribution could be tailored to alleviate adverse forces or even possibly to generate favorable forces on the boom section and minimize the area requiring venting. The idea was to connect areas of relatively high and low pressures so that these areas would communicate. For example, if an area of relatively high pressure near the windward section of the boom was connected to a side area with relatively low pressure, the high pressure area causing additional down load would be reduced and the lower pressure side area causing a side force (and yawing moment) would also be reduced. Therefore, the net result might be a reduction in both down load and adverse side force. Pressure distributions of the oval-shaped boom without porosity are contained in reference 2. The oval boom was tested more extensively than the trapezoidal boom, since the oval shape was representative of a currently used (UH-60) tail boom shape.

This investigation was conducted in the Langley 14- by 22-Foot Subsonic Tunnel in the closed test section configuration. A comprehensive description of the tunnel and associated hardware is described in reference 7. A sketch of the test apparatus and the reference area used in calculation of the aerodynamic coefficients is shown in figures 2(b) and 3(a). Photographs of the installation of the model in the test section of the 14-by 22-Foot Subsonic Tunnel and of the internal construction of the model metric section are also shown in figures 3(b) and 3(c).

Test Procedures and Accuracy

Data for the two boom shapes were first obtained at three constant angles of incidence (0°, 10°, and 20°) with the free-stream dynamic pressure varying from 1 to 30 psf to identify any Reynolds number dependence of the aerodynamic characteristics for the two shapes. This range covered the ranges of Reynolds numbers (Re) seen by full-scale helicopters during hover and crosswind flight conditions where boom loading can be a significant problem. Data were then obtained at three constant dynamic pressures (10, 20, and 25 psf)

with the angle of incidence ϕ varying in increments from $-90°$ to $90°$. This range covered the incidence angles and Reynolds numbers that a typical tail boom would experience due to main rotor downwash and free-stream flow during hover and left and right sideward flight. The test data were not corrected for blockage effects, since the volume of the test apparatus was considered significantly smaller than the test section volume based on classical analysis (ref. 8) and only incremental data were desired.

The accuracy of the strain-gauge balance was reported to be ±1.25 lbf in both normal force and side force with all the beams fully loaded. The repeatability of these measurements during the current and previous investigations with this setup was approximately ±0.20 lbf. This repeatability is partly caused by the balance being relatively lightly loaded in most axes; this equates to a normal and side force coefficient accuracy of ±0.003 and repeatability of ±0.001 at $q_\infty = 20$ psf.

Because of the increase in surface roughness caused by the design and manufacture of the porous skin, that is, holes larger than necessary for the skin thickness (ref. 5), the normal force may be increased relative to a porous surface with proper hole size.

Data Analysis

Calculations of full-scale tail boom normal force (down load) and side force were made by using the model force coefficients at an incidence angle of 15°. An incidence angle of 15° was used because it is the approximate stall angle for the solid, baseline, oval shape (ref. 2) and simulates a right sideward flight condition where the boom side force would be close to maximum in a direction that increases the demand on the tail rotor horsepower. The effectiveness of venting and strakes would likely have the largest payoff in terms of yaw control and performance at this condition. Characteristics for a full-scale UH-60 were used for data calculations. Average downwash dynamic pressure q at the tail boom was 5.2 psf. Reference areas (vertically projected area S) for the UH-60 tail boom and the trapezoidal-shaped tail boom attached to the UH-60 were 29.7 ft^2 and 24.2 ft^2, respectively. Standard sea-level air density, 0.002378 slugs/ft^3, was used. The projected area of the trapezoidal-shaped boom was less because the model was narrower than the oval-shaped model (10.2 in. versus 12.5 in.). Therefore, qS for the oval shape (154.4 lbf full scale) and qS for the trapezoidal shape (126.0 lbf full scale) were constant for their respective (oval or trapezoidal) calculations. The distance from the aircraft center of gravity (assumed to be located on the main rotor shaft centerline) to the aerodynamic center of the tail boom and from the center of gravity to the tail rotor center of rotation were assumed to be 19.7 ft and 32.6 ft, respectively. The main rotor was assumed to offset the boom down load with a lift capability of 8 lbf/hp. The net yawing moment generated by the tail boom was balanced by an assumed tail rotor thrust capability of 4 lbf/hp. An example of the calculation for the oval cross section is given as follows:

$$N_B = c_z qS = (-0.119)(154.4 \text{ lbf}) = -18.4 \text{ lbf}$$

(Note that for some conditions the down load is negative, that is, a favorable lifting force.)

$$\text{HP}_{\text{DL}} = -\frac{-18.4 \text{ lbf}}{8 \text{ lbf/hp}} = +2.3 \text{ hp}$$

$$Y_B = c_y qS = (-1.543)(154.4 \text{ lbf}) = -238.2 \text{ lbf}$$

The side force acting at the tail boom aerodynamic center is 19.7 ft from the aircraft center of gravity, and the tail rotor thrust required to offset this side force Y_B is applied at 32.6 ft from the aircraft center of gravity. The tail rotor thrust to counteract the yawing moment from Y_B is

$$Y_T = \frac{(-238.2 \text{ lbf})(19.7 \text{ ft})}{32.6 \text{ ft}} = -144 \text{ lbf}$$

at tail rotor center of rotation to counteract boom yawing moment

$$\text{HP}_{\text{SL}} = \frac{-144 \text{ lbf}}{4 \text{ lbf/hp}} = -36.0 \text{ hp}$$

Two-dimensional data are being used to calculate three-dimensional results, and a number of assumptions are being made such as

(1) The use of an average value of main rotor downwash dynamic pressure along the tail boom

(2) Estimating the location of the aerodynamic center on the boom

(3) Estimating the location of the aircraft center of gravity as being directly under the main rotor centerline

(4) The main and tail rotors would produce 8 lbf thrust/hp and 4 lbf thrust/hp, respectively

Only the trends of the calculated horsepower and not the absolute values are believed to be meaningful.

Presentation of Results

The measured force results are presented in plots showing normal force and side force coefficients c_z and c_y as a function of dynamic pressure q_∞ or incidence angle ϕ. Calculated horsepower required to overcome adverse normal and side forces are presented after the force coefficient data. The values of c_y and c_z are based on the convention shown in figure 2. The figures are presented as follows:

The calculated results in terms of horsepower required to trim tail boom loads are also presented numerically for the various configurations in tables 1 through 8.

Discussion of Results

Effect of (Re) Dynamic Pressure on Fully Porous Booms

The effect of dynamic pressure q_∞ and incidence angle ϕ on the oval cross section and the trapezoidal cross-section boom shapes is presented in figures 6 and 7, respectively. Figures 6(a) and 7(a) present the c_z and c_y characteristics for each configuration plotted against q_∞ for three values of ϕ (0°, 10°, and 20°) representative of hover and sideward flight conditions. Figures 6(b) and 7(b) present similar data for the entire range of ϕ examined during this investigation (−90° to +90°). Figures 6(c) and 7(c) present the c_z and c_y characteristics plotted against ϕ. Most data in this investigation were obtained at q_∞ values of 10, 20, and 25 psf because these values bracketed representative free-stream conditions typically experienced by the boom in hover and sideward flight.

Oval Configuration

The effect of varying q_∞ on c_y and c_z for the fully porous oval tail boom shape is shown in figure 6. The results of figure 6(a) show that there is an increase in c_z and a decrease in c_y (ϕ = 10° and 20°) for the oval boom when q_∞ is reduced below 5 psf but very little changes above 5 psf. The results from figures 6(b) and 6(c) indicate that there is very little change in c_y (at fixed ϕ) with q_∞ for $q_\infty \geq 5$ and very little change in c_z (at fixed ϕ) with q_∞ for $q_\infty \geq 10$ psf.

Trapezoidal Configuration

The effect of q_∞ and ϕ on the c_y and c_z from the trapezoidal boom is shown in figure 7. A much greater increase occurs in c_z and c_y as q_∞ is reduced. Most of the effects for the trapezoidal cross section are seen for values of q_∞ up to 10 psf. Also, figure 7(a) shows a nonzero c_y at ϕ = 0° for the trapezoidal boom, indicating that the model shape is not symmetrical. Figures 7(b) and 7(c) show that although there appears to be little change in c_y for all ϕ angles at q_∞ from 5 to 30 psf, there were significant changes in c_z. The changes in c_z are not symmetrical at positive and negative ϕ angles (fig. 7(c)). These changes again indicate an asymmetry in the shape of the model. The trapezoidal model had rounded corners and it is speculated that this probable geometric asymmetry (manufacturing deviation) resulted in one windward (top) side having a larger effective radius than the other; thereby, flow separation was delayed on that corner compared with the other. Another possibility is that the TRDSC may not be symmetric (manufacturing deviation); thereby, separation is promoted in one direction of flow and not the other.

Effect of Venting Area and Location

Various venting schemes were tried during this investigation. These venting schemes were accomplished by taping over the fully porous models to simulate solid areas of the boom and to produce desired venting configurations. The various configurations are shown in figure 5.

Symmetric Configurations

The effects of venting area and location on the boom aerodynamics are presented in figure 8 for the oval boom model (q_∞ = 20 and 25 psf and 10 psf). The five configurations that are shown, in order of increasing ventilation, are fully solid baseline (O1), 1/4 side vented (O2), 1/2 side vented (O3), all except the TRDSC vented (O4), and fully porous (O5). The effect of increasing venting is a reduction in the slope of the curve for c_y versus ϕ (reduced side force sensitivity) at $-15° < \phi < 15°$ and a smoother transition through stall as ϕ increases above 15°. The baseline (O1) data curve has an abrupt change in slope at $\phi = \pm 15°$ which is attributed to stall of the boom shape (ref. 2). The smooth transition indicates that the boom with fully porous venting (O5) does not stall in the test range of ϕ. The configurations with reduced areas of venting (O2, O3, and O4) do stall but not as abruptly as the solid baseline (O1). This result would also imply that aircraft unsteadiness which could be caused in flight by partially and fully separated flow fields near and beyond tail boom stall are mitigated. This effect was qualitatively observed during the test, although no dynamic data were obtained during this investigation. The controllability and unsteadiness in hover and sideward flight of helicopters can be a significant problem at certain crosswind angles (ref. 9). The absence of abrupt stall and unsteadiness can be a significant improvement resulting from the boom design in conjunction with reductions in adverse boom side force to reduce the tail rotor horsepower required.

An increase in c_z occurred with increased venting at $-35° < \phi < 35°$, but a decrease in c_z occurred at higher values of $|\phi|$. This increase is thought to occur, at least in part, because of the increase of the surface roughness caused by the porous surface but primarily because of improper sizing of the hole diameter to skin thickness. As is shown by calculations later, even with the less than optimized material, the benefits derived in a reduction of side force more than make up for the increases in down load on a total or net horsepower basis. Additionally, the helicopter main rotor is roughly twice as efficient as the tail rotor in terms of lift per horsepower where the main rotor will produce about 8 lbf of lift/hp and the tail rotor will produce about 4 lbf thrust/hp.

Simple calculations using the two-dimensional c_y and c_z data at $\phi = +15°$ for a UH-60 helicopter were made with assumed locations for the aircraft longitudinal center of gravity (main rotor shaft centerline), aerodynamic center of the boom (19.7 ft rearward of the center of gravity), the tail rotor centerline distance from the center of gravity (32.6 ft), and the reference area of the tail boom (29.7 ft^2). The vertical area was used because the two-dimensional coefficient data were referenced to that area by using the convention shown in figure 2(b). The dynamic pressure q at the tail boom was calculated by using $\rho = 0.002378$ slugs/ft^3 (standard sea level density) and a wake velocity of 66 ft/sec at the boom. Calculations were made at $\phi = 15°$ because at that angle c_y is maximum just prior to the stall angle for the oval shape in right sideward flight.

The calculated costs in horsepower for boom down load, side force, net cost (down load plus side force), and the total horsepower saved compared with the solid oval baseline shape (O1) were calculated for each configuration to show relative gains and losses associated with all the configurations investigated. The results are presented in figure 9 and table 1. The calculated cost in down load penalty in going from the solid configuration (O1) to the fully porous configuration (O5) is 16.2 hp and the gain in tail rotor horsepower due to the tail boom side force change is 26.0 hp with a 9.8 hp net gain (on the order of 0.5 percent of total power required to hover). The reduction of 26 hp for the tail rotor represents a reduction in tail rotor power on the order of about 10 percent. This is roughly a 1.6-to-1 (26/16.2) net gain; but perhaps more importantly, a sizeable reduction is realized in the amount of yaw control required. In general, the results in figure 9 (table 1) indicate that the fully porous configuration (O5) would be the most effective in reducing the tail rotor horsepower required to overcome boom side force, but configurations O3 and O4 result in comparable levels of required power (10.0 hp versus 12.1 hp). All the configurations are close on the basis of net power saved relative to the solid baseline, O1 (range from 9.0 to 10.6 hp).

The effect of symmetric venting and location on the force coefficients of the trapezoidal-shaped tail boom is shown in figure 10. Similar characteristics that were previously described for the oval-shaped boom are seen for the trapezoidal boom shape. However, the addition of venting has a relatively small effect on the down load at $\phi = 0°$. This effect is in contrast to the large increases in down load associated with the addition of venting for the oval case, perhaps because initially the solid trapezoidal shape has a high down load at $\phi = 0°$. The vented configurations (T2, T3, T4, and T5) show smoother variations in down load with increases in ϕ than the solid configuration (T1); this would be consistent with flow separation occurring downstream of the upper corners. The benefits in terms of reduction of the slope of c_y versus ϕ are still realized, although not as dramatic as seen with the oval boom configurations. The mitigation of the abrupt stall is still seen at incidence angles between about 15° and 45° with the vented configurations (T2, T3, T4, and T5) as compared with the solid baseline (T1). This mitigation would indicate a benefit in both the static performance (tail rotor power required and total power required) as well as the dynamic controllability of a full-scale helicopter using this boom design.

Calculations made for the trapezoidal shape, presented in figure 11, scaled up to a UH-60 helicopter boom, yield similar results in terms of power (net) savings for the respective porous configurations compared with the solid baseline configurations O1 and T1 (9.8 hp for oval and 12.4 hp for the trapezoidal shape). The data in figure 11 and table 2 indicate that the porous trapezoidal shape (T5) is best from a side force standpoint (−16.0 hp required to trim with a reduction of 28.4 hp relative to the solid trapezoidal baseline which required 44.4 hp to trim) and most of the trapezoidal configurations are close for overall power saved relative to the solid trapezoid (T1).

Asymmetric Configurations

The effect of asymmetric porosity distribution on the section force coefficients for the oval shape is shown in figure 12. The asymmetric configurations were investigated to determine the ability of venting to modify the overall pressure distribution in a beneficial manner by communicating areas of high pressure to those with low pressure. The asymmetric venting configurations were only tested on the oval boom shape. The specific purpose of the asymmetry was to try to reduce the adverse forces on the boom by shifting c_y in a favorable direction (more positive) and to see if smaller areas of venting (porosity) would produce a major portion of the desirable effects of full porosity without the adverse effects of increased down load. The shifting in c_y is accomplished by tailoring the pressure distribution between the two sides through various venting schemes. The low asymmetric configuration (O6) resulted in a slight shift of the curve for c_y versus ϕ, a slight reduction in slope, and an increase in down load from $c_z = 0.3$ to 0.77 at $\phi = 0°$. The coefficient c_z was identical to the one for the porous configuration (O5) at $\phi = 0°$ but quickly reduces for $|\phi| > 0°$ for angles in the normal range of operation ($-45° < \phi < 45°$). The high asymmetric configuration (O7) showed a similar slope for c_y versus ϕ to that of the low asymmetric configuration (O6) with a favorable shift of the side force curve similar to the shift found with strakes in reference 2. The value of c_z was about midway between the value of c_z for the solid baseline (O1) and fully porous (O5) at $\phi = 0°$, decreased with increasing ϕ, and eventually increased to a value close to the value of the porous configuration (O5) near $\phi \approx 45°$. Data are very similar for $q_\infty = 20$ and 25 psf (fig. 12(a)) and 10 psf (fig. 12(b)).

Results from calculations of the horsepower required to balance the tail boom aerodynamic forces using the two-dimensional model coefficients at $\phi = 15°$ (fig. 12) are given in figure 13 and table 3. The high asymmetric configuration (O7) required less power to balance the adverse boom side force as well as significantly lower net power (to trim down load and side force) compared with the solid baseline configuration (O1). In a net power sense, the high asymmetric configuration (O7) was about 50 percent better than the solid baseline (O1), and the low asymmetric (O6) and fully porous (O5) configurations were 15 and 24 percent better than the solid baseline (O1), respectively. These trends indicate that the high asymmetric configuration (O7) is superior to both the low asymmetric (O6) and the fully porous (O5) configurations.

Effect of Venting in Combination With Strakes

Symmetric Configurations

In previous research, strakes have been shown to separate the attached flow on one side of the tail boom and reduce the adverse c_y; therefore, the tail rotor power requirement is reduced and yaw control margin, particularly in right sideward flight, is increased. (See refs. 2, 3, and 9.) Using venting in combination with the strakes could have a beneficial combined effect on the side force and down load characteristics. The oval boom was tested with both single (S1 and S2) and double strakes (S2S3) on the baseline solid (O1), full porosity venting (O5), and some limited combination of strakes on the asymmetric configurations (O6 and O7). The trapezoidal boom was tested only with single strake (S4) but with several combinations of symmetric venting schemes. The effect of boom strakes in combination with symmetric venting schemes on the normal and side force coefficients is shown for the oval boom in figure 14 and for the trapezoidal boom in figure 16. In most cases, the effect of strakes was similar to the effect of venting; that is, the strakes created a favorable shift toward positive c_y but also created an increase in down load c_z in the region of $0° < \phi < 45°$. This trade-off between side force benefit and down load penalty is considered beneficial, since there is a significant improvement in yaw control, an attendant decrease in tail rotor power, and a net power benefit. For these configurations in a two-dimensional flow environment, the double strakes appear to produce nearly the same effect as that of the single upper strake as tested on the oval tail boom. Flight tests (ref. 9) have shown that with three-dimensional flow there is an added benefit of the second strake.

Calculated values of horsepower required to overcome the boom aerodynamic forces for the configurations of figure 14(a) and figure 16 at $\phi = 15°$ are given in figures 15 and 17 and tables 4 and 5. For the oval-shaped boom, the solid configuration with the double 2-in-high strakes (O1S2S3) is the best from a standpoint of tail rotor power saved (+9.3 hp) and from total power saved (21.6 hp) compared with the solid baseline oval shape (O5). For the trapezoidal-shaped boom (fig. 17), the solid with 1.5-in. single strake (T1S4)

and 1/4 solid with a 1.5-in. strake (T3S4) were the best from a standpoint of side force power required (10.8 hp). The solid with single 1.5-in. strake (T1S4) was the best from a standpoint of net power saved relative to the solid baseline trapezoid (T1); however, all configurations were fairly close in terms of HP_{DL}, HP_{SL}, and HP_{net}.

Asymmetric Configurations

The oval boom was tested with a combination of asymmetric venting and strakes to determine if there could be a beneficial combined effect and the results are shown in figure 18 and figure 19 and table 6. The effect of adding a single strake is similar to that seen for the full porous venting schemes (O5) with strakes and that seen with the solid baseline (O1) with strakes, that is, a positive shift of the c_y and an increase in c_z in the region $0° < \phi < 45°$. As with the fully porous venting scheme (O5), the effect of adding the second lower strake on the low asymmetric configurations (O6) was not significant in the region of most interest ($-15° < \phi < 45°$). The effect of adding strakes on the high asymmetric configuration (O7) was slightly less than it was for the low asymmetric configuration (O6) in terms of HP_{saved} (1.9 hp). However, the high asymmetric configuration without strakes was still superior to the low asymmetric configuration with strakes and was able to realize an additional benefit from the strakes. The high asymmetric configuration with strakes was the best configuration tested in terms of HP_{saved} (22.3 hp).

Calculations of the effects of the addition of strakes on the aerodynamics of the asymmetric venting configurations (O6 and O7) in terms of horsepower required to trim the boom forces are given in figure 19 and table 6. The high asymmetric configuration with a single 1.5-in. strake (O7S1) was clearly the best for HP_{SL} (+7.0 hp or 43 hp less than the solid baseline) and for HP_{saved} (22.3 hp).

Figure 20 and table 7 present a summary of the results for the oval shape. Overall, of all the oval configurations at $\phi = 15°$, the solid baseline oval with the double 2-in. strakes (O1S2S3) was the best from a side force standpoint (+9.3 hp), while the high asymmetric with a single 1.5-in. strake (O7S1, +7.0 hp) and the solid baseline oval with a single 2-in. strake (O1S2, +6.5 hp) each performed almost as well. For net power saved relative to the solid oval baseline (O1), the best configurations were the high asymmetric with the single 1.5-in. strake (O7S1, 22.3 hp), solid with double 2-in. strakes (O1S2S3, 21.6 hp), solid baseline with single 2-in. strakes (O1S2, 18.2 hp), and high asymmetric (O7, 16.9 hp).

Figure 21 and table 8 present a summary of the results for the trapezoidal shape. The best overall trapezoidal configurations, evaluated at $\phi = 15°$, were the solid baseline with 1.5-in. strake (T1S4, 10.8 HP_{SL} and 14.7 HP_{net} decreased relative to the solid trapezoidal baseline, T1), the 1/4 solid with single 1.5-in. strake (T3S4, 10.8 HP_{SL} and 13.2 HP_{net} decreased relative to the solid trapezoid baseline, T1), and the porous trapezoid (T5, 16.0 HP_{SL} and 12.4 HP_{net} decreased relative to the solid trapezoid baseline, T1).

Summary of Results

An exploratory investigation was conducted to determine the effectiveness of passively venting a helicopter tail boom model to reduce side force and down load during simulated hover and sideward flight conditions. A two-dimensional tail boom model with two different cross-sectional shapes was used. One was an oval cross-sectional shape representative of a UH-60 tail boom, and the other was a trapezoidal cross section representative of a low-observable tail boom. The models were 1/2-scale cross sections of the mid boom. Various venting schemes were investigated with a porous skin. The porous skin was partially covered in some cases to simulate venting in various locations as well as the completely solid (totally covered) and completely porous cases. Some of the venting schemes were also investigated in conjunction with single and double strakes. Section side force and normal force coefficients c_y and c_z were obtained on each configuration at angles of incidence ϕ from $-90°$ to $+90°$. Calculations were made by using the coefficients at $\phi = 15°$ (approximate stall angle for solid oval boom) to determine the approximate trends of the boom aerodynamics in terms of power required to balance side force and down load if these booms were installed on a UH-60 size helicopter.

The results indicate that passive venting can reduce a significant portion of the adverse side force created on the tail boom at conditions representative of hover and sideward flight. Most of the venting schemes created additional down load at low

incidence angles, but this is thought to be partly due to the additional skin friction created by the porous skin used. By using a porous skin more optimally designed for this purpose or by employing venting schemes that do not use a porous surface, it may be possible to gain the benefits of venting in side force benefits with minimal increases in down load.

No asymmetric configurations were tested on the trapezoidal-shaped tail boom. It was apparent from the oval results that the asymmetric configurations were the best overall vented configurations and the only ones that compared favorably to the solid strake configurations. No symmetric venting configuration on the trapezoidal-shaped tail boom, including in combination with strakes, performed better than the solid trapezoidal configuration with strakes.

Based on the calculated trends (ϕ = 15°) of the oval configurations investigated, the following results are given:

1. Configuration O1S2S3, the solid tail boom configuration with double 2-in. strakes, was the best configuration from a side force standpoint (tail rotor power reduction of +9.3 hp).

2. Configuration O7S1, the high asymmetric with a single 1.5-in. strake (tail rotor power reduction of +7.0 hp), and configuration O1S2, the solid with a single 2-in. strake (tail rotor power reduction of +6.5 hp), both performed almost as well.

3. The best overall configurations (total power saved) were the high asymmetric with the single 1.5-in. strake (22.3 hp saved), solid with double 2-in. strakes (21.6 hp saved), solid with a single 2-in. strake (18.2 hp saved), and high asymmetric with no strake (16.9 hp saved).

References

1. Sampatacos, E. P.; Morger, K. M.; and Logan, A. H.: NOTAR—The Viable Alternative to a Tail Rotor. AIAA-83-2527, 1983.

2. Wilson, John C.; and Kelley, Henry L.: *Aerodynamic Characteristics of Several Current Helicopter Tail Boom Cross Sections Including the Effect of Spoilers.* NASA TP-2506, AVSCOM TR 85-B-3, 1986.

3. Crowell, Cynthia A.; and Kelley, Henry L.: *Aerodynamic Effect of Strakes on Two-Dimensional Tail Boom Models of the OH-58A and the OH-58D Helicopters.* NASA TM-4248, AVSCOM TR-90-B-010, 1990.

4. Lockwood, Roy A.; Kelly, William A.; and Cason, Randall W.: *Flight Characteristics Test of the UH-60A With Tail Boom Mounted Strake.* USAAEFA Proj. No. 85-07, U.S. Army, Oct. 1986.

5. Bauer, Steven X. S.; and Hernandez, Gloria: Reduction of Crossflow Shock-Induced Separation With a Porous Cavity at Supersonic Speeds. AIAA-88-2567, 1988.

6. Bauer, S. X. S.; and Hemsch, M. J.: Alleviation of Side Force on Tangent-Ogive Forebodies Using Passive Porosity. *J. Aircr.*, vol. 31, no. 2, 1994, pp. 354–361.

7. Gentry, Garl L., Jr.; Quinto, P. Frank; Gatlin, Gregory M.; and Applin, Zachary T.: *The Langley 14-by 22-Foot Subsonic Tunnel—Description, Flow Characteristics, and Guide for Users.* NASA TP-3008, 1990.

8. Rae, William H., Jr.; and Pope, Alan: *Low-Speed Wind Tunnel Testing*, second ed. John Wiley & Sons, Inc., 1984.

9. Kelley, Henry L.; Crowell, Cynthia A.; Yenni, Kenneth R.; and Lance, Michael B.: *Flight Investigation of the Effect of Tail Boom Strakes on Helicopter Directional Control.* NASA TP-3278, ATCOM TR-93-A-003, 1993.

Table 1. Power Costs for Oval Boom, Symmetric Configurations With q_∞ = 20 and 25 psf

Configuration	HP_{DL} at $\phi = 15°$	HP_{SL} at $\phi = 15°$	HP_{net}, $HP_{DL} + HP_{SL}$	HP_{saved} relative to baseline
Solid baseline, O1	+2.3	−36.0	−33.7	
1/2 side porous, O2	−6.0	−18.7	−24.7	9.0
Porous sides, O3	−11.0	−12.1	−23.1	10.6
Porous, solid TRDSC, O4	−11.8	−12.1	−23.9	9.8
Porous, O5	−13.9	−10.0	−23.9	9.8

Table 2. Power Costs for Trapezoidal Boom, Symmetric Configurations With q_∞ = 20 and 25 psf

Configuration	HP_{DL} at $\phi = 15°$	HP_{SL} at $\phi = 15°$	HP_{net}, $HP_{DL} + HP_{SL}$	HP_{saved} relative to baseline
Solid trapezoidal baseline, T1	+3.9	−44.4	−40.5	
1/2 solid, T2	−4.3	−28.2	−32.5	+8.0
1/4 solid, T3	−7.6	−21.5	−29.1	+11.4
Porous, solid TRDSC, T4	−9.0	−19.0	−28.0	+12.5
Porous, T5	−12.1	−16.0	−28.1	+12.4

Table 3. Power Costs for Oval Boom, Asymmetric Configurations With q_∞ = 20 and 25 psf

Configuration	HP_{DL} at $\phi = 15°$	HP_{SL} at $\phi = 15°$	HP_{net}, $HP_{DL} + HP_{SL}$	HP_{saved} relative to baseline
Solid oval baseline, O1	+2.3	−36.0	−33.7	
Low asymmetric, O6	−5.2	−23.3	−28.5	+5.2
High asymmetric, O7	−7.9	−8.9	−16.8	+16.9
Porous, O5	−13.9	−10.0	−23.9	+9.8

Table 4. Power Costs for Oval Boom, Strake Configurations With q_∞ = 20 psf

Configuration	HP_{DL} at $\phi = 15°$	HP_{SL} at $\phi = 15°$	HP_{net}, $HP_{DL} + HP_{SL}$	HP_{saved} relative to baseline
Solid oval baseline, O1	+2.3	−36.0	−33.7	
Solid + double 2-in. strakes, O1S2S3	−21.4	+9.3	−12.1	+21.6
Solid + single 2-in. strake, O1S2	−22.0	+6.5	−15.5	+18.2
Porous + double 2-in. strakes, O5S2S3	−22.8	−3.4	−26.2	+7.5
Porous + single 2-in. strake, O5S2	−22.8	−3.4	−26.2	+7.5
Porous, O5	−13.9	−10.0	−23.9	+9.8

Table 5. Power Costs for Trapezoidal Boom, Strake Configurations With q_∞ = 20 and 25 psf

Configuration	HP_{DL} at $\phi = 15°$	HP_{SL} at $\phi = 15°$	HP_{net}, $HP_{DL} + HP_{SL}$	HP_{saved} relative to baseline
Solid trapezoidal baseline, T1	+3.9	–44.4	–40.5	
Porous + single 1.5-in. strake, T5S4	–17.6	–11.3	–28.9	+11.6
Solid TRDSC + single 1.5-in. strake, T4S4	–15.4	–12.1	–27.5	+13.0
1/4 solid + single 1.5-in. strake, T3S4	–16.5	–10.8	–27.3	+13.2
1/2 solid + single 1.5-in. strake, T2S4	–15.6	–12.2	–27.8	+12.7
Solid + single 1.5-in. strake, T1S4	–15.0	–10.8	–25.8	+14.7

Table 6. Power Costs for Oval Boom, Asymmetric and Strake Configurations With q_∞ = 20 and 25 psf

Configuration	HP_{DL} at $\phi = 15°$	HP_{SL} at $\phi = 15°$	HP_{net}, $HP_{DL} + HP_{SL}$	HP_{saved} relative to baseline
Solid oval baseline, O1	+2.3	–36.0	–33.7	
Low asymmetric, O6	–5.2	–23.3	–28.5	+5.2
Low asymmetric + single 2-in. strake, 0O6S2	–21.2	0	–21.2	+12.5
Low asymmetric + double 2-in. strakes, O6S2S3	–21.2	0	–21.2	+12.5
High asymmetric, O7	–7.9	–8.9	–16.8	+16.9
High asymmetric + single 1.5-in. strake, O7S1	–18.4	+7.0	–11.4	+22.3

Table 7. Summary of Results for Oval Boom

Configuration	HP_{DL} at $\phi = 15°$	HP_{SL} at $\phi = 15°$	HP_{net}, $HP_{DL} + HP_{SL}$	HP_{saved} relative to baseline
Solid oval baseline, O1	+2.3	−36.0	−33.7	
Porous, O5	−13.9	−10.0	−23.9	9.8
High asymmetric, O7	−7.9	−8.9	−16.8	16.9
High asymmetric + single 1.5-in. strake, O7S1	−18.4	+7.0	−11.4	22.3
Solid oval + single 2-in. strake, O1S2	−22.0	+6.5	−15.5	18.2
Solid oval + double 2-in. strakes, O1S2S3	−21.4	+9.3	−12.1	21.6

Table 8. Summary of Results for Trapezoidal Boom

Configuration	HP_{DL} at $\phi = 15°$	HP_{SL} at $\phi = 15°$	HP_{net}, $HP_{DL} + HP_{SL}$	HP_{saved} relative to baseline
Solid trapezoid, T1	+3.9	−44.4	−40.5	
Porous trapezoid, T5	−12.1	−16.0	−28.1	12.4
1/4 solid + single 1.5-in. strake, T3S4	−16.5	−10.8	−27.3	13.2
Solid + single 1.5-in. strake, T1S4	−15.0	−10.8	−25.8	14.7

Figure 1. UH-60 helicopter.

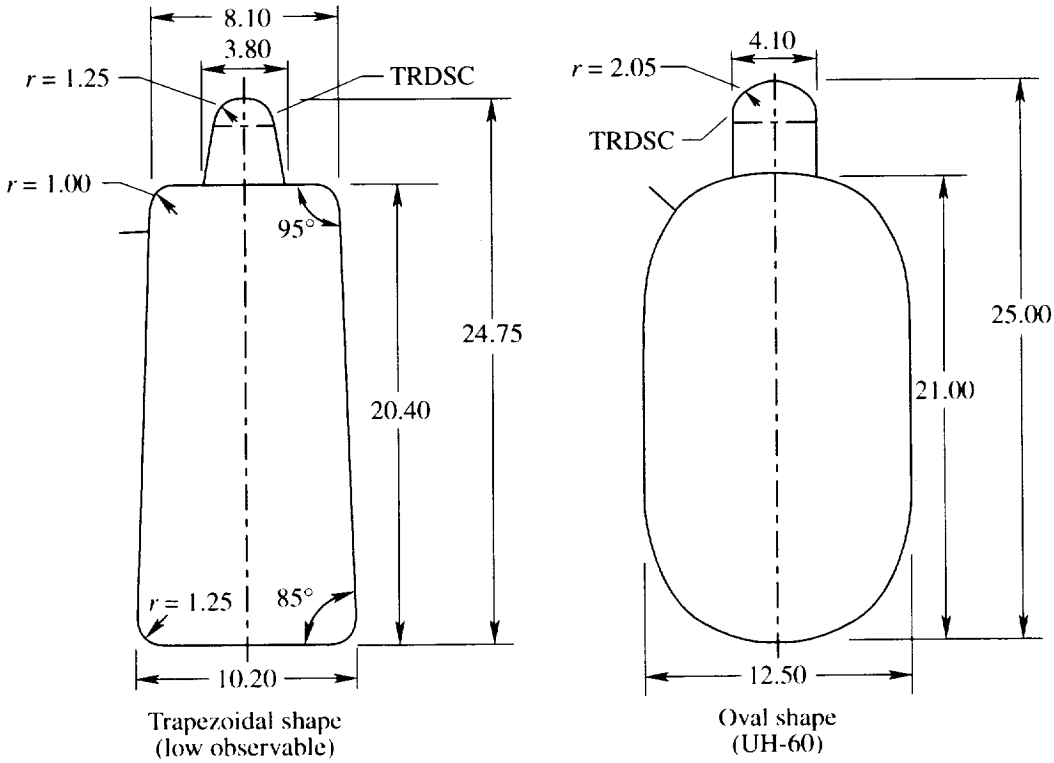

(a) Sketches; linear dimensions are in inches.

Figure 2. Model sketches and photographs.

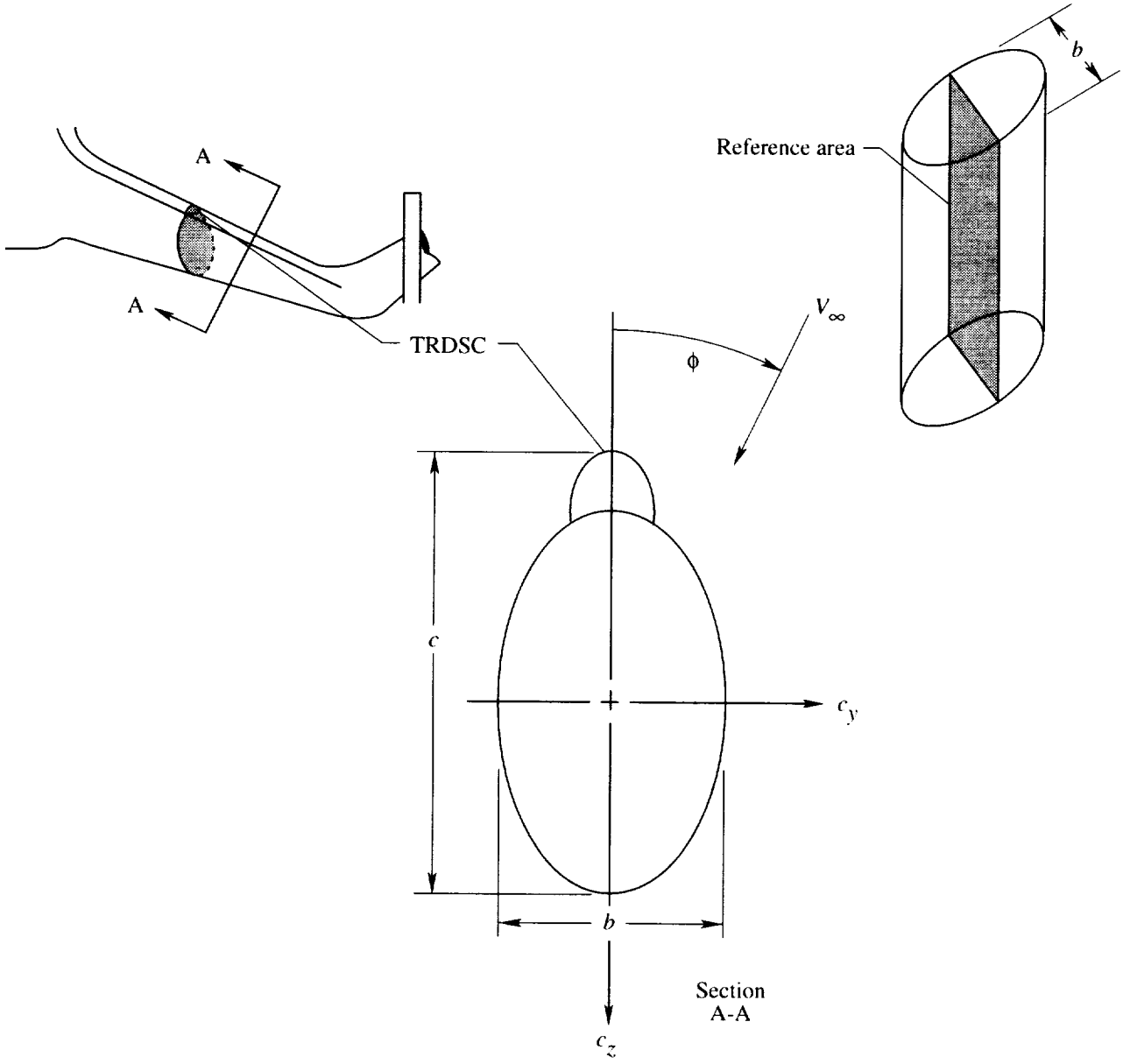

(b) Conventions for model incidence, reference dimensions, and coefficients.

Figure 2. Continued.

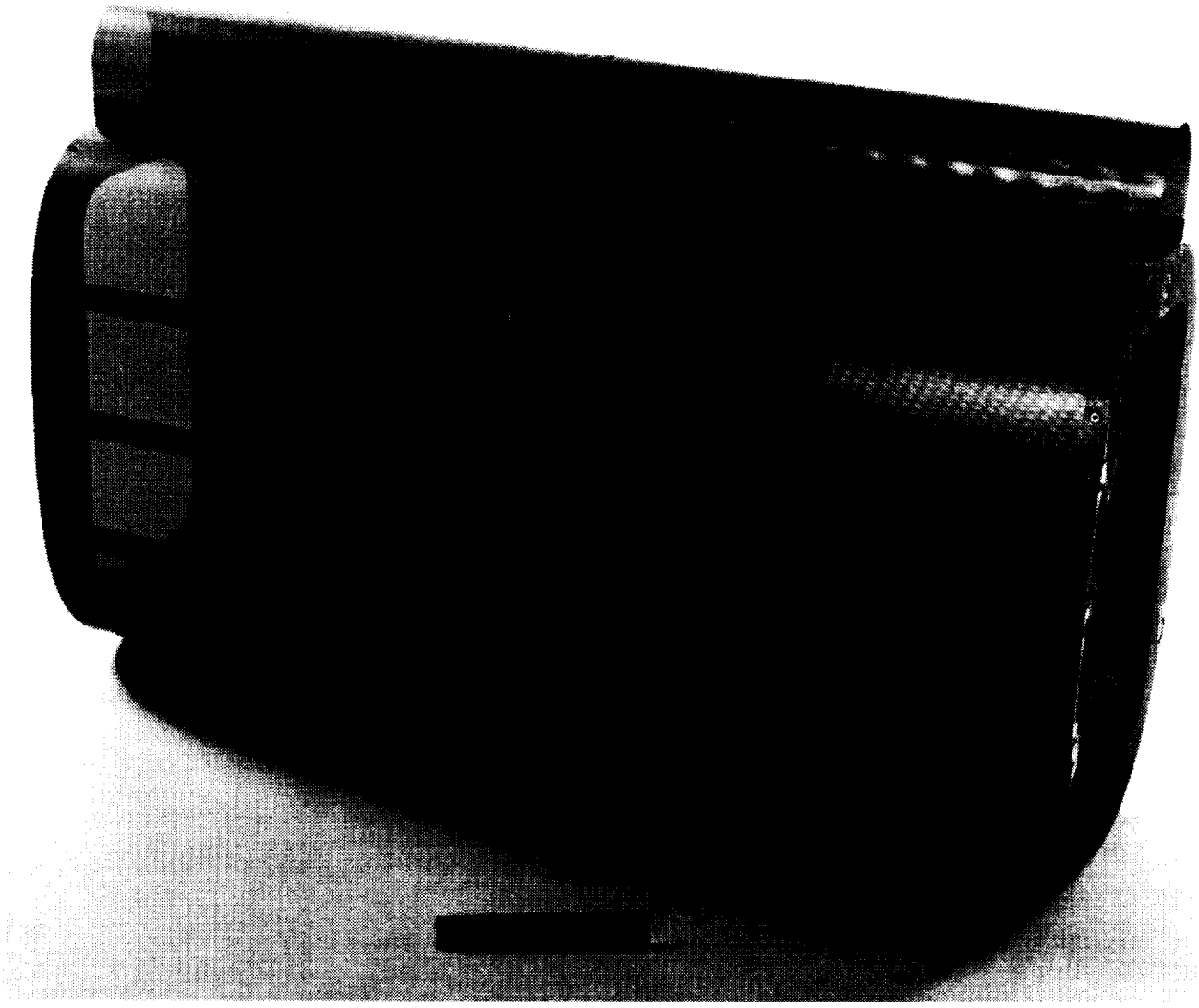

(c) Oval-shaped boom.

Figure 2. Continued.

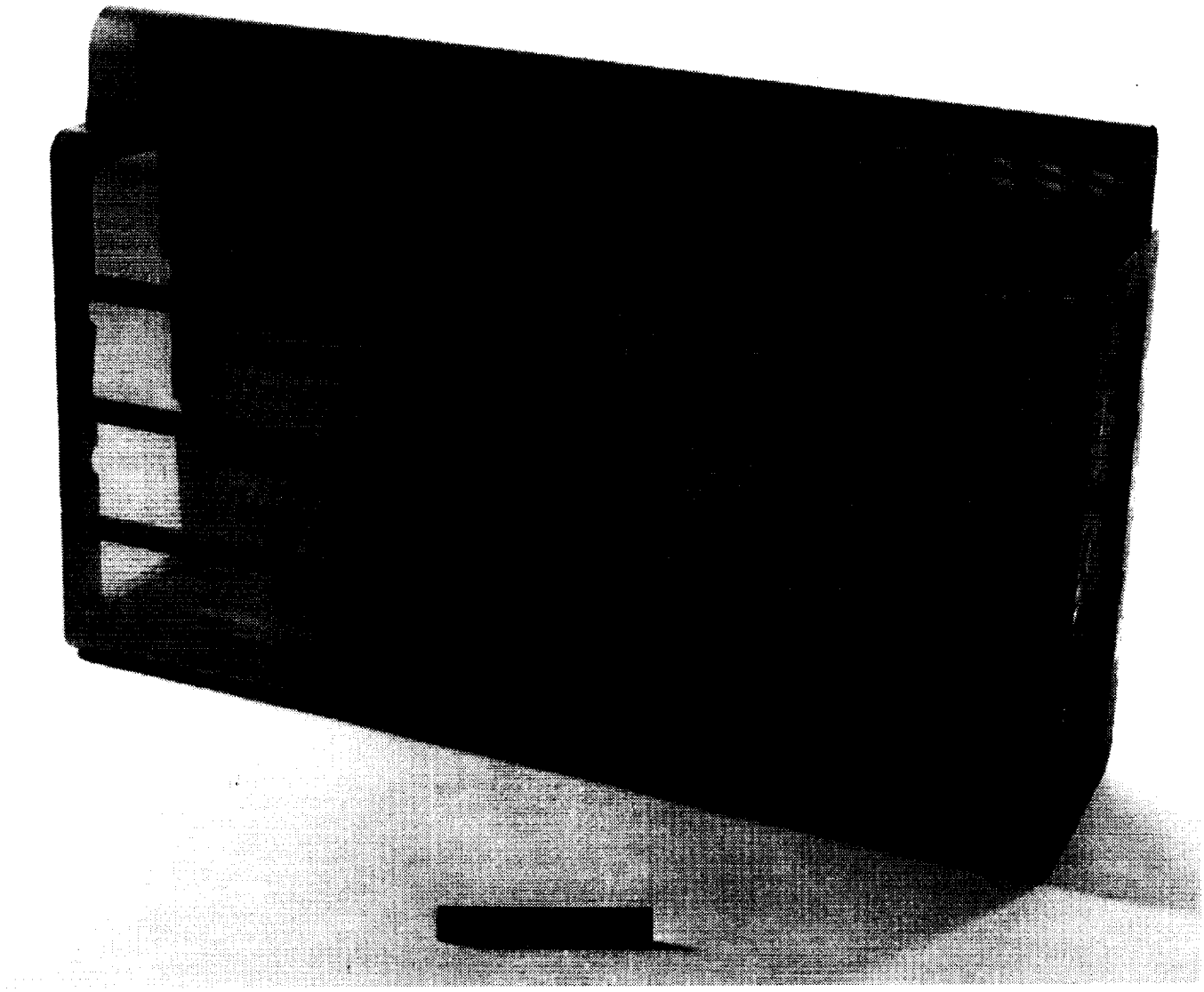

(d) Trapezoidal-shaped boom.

Figure 2. Concluded.

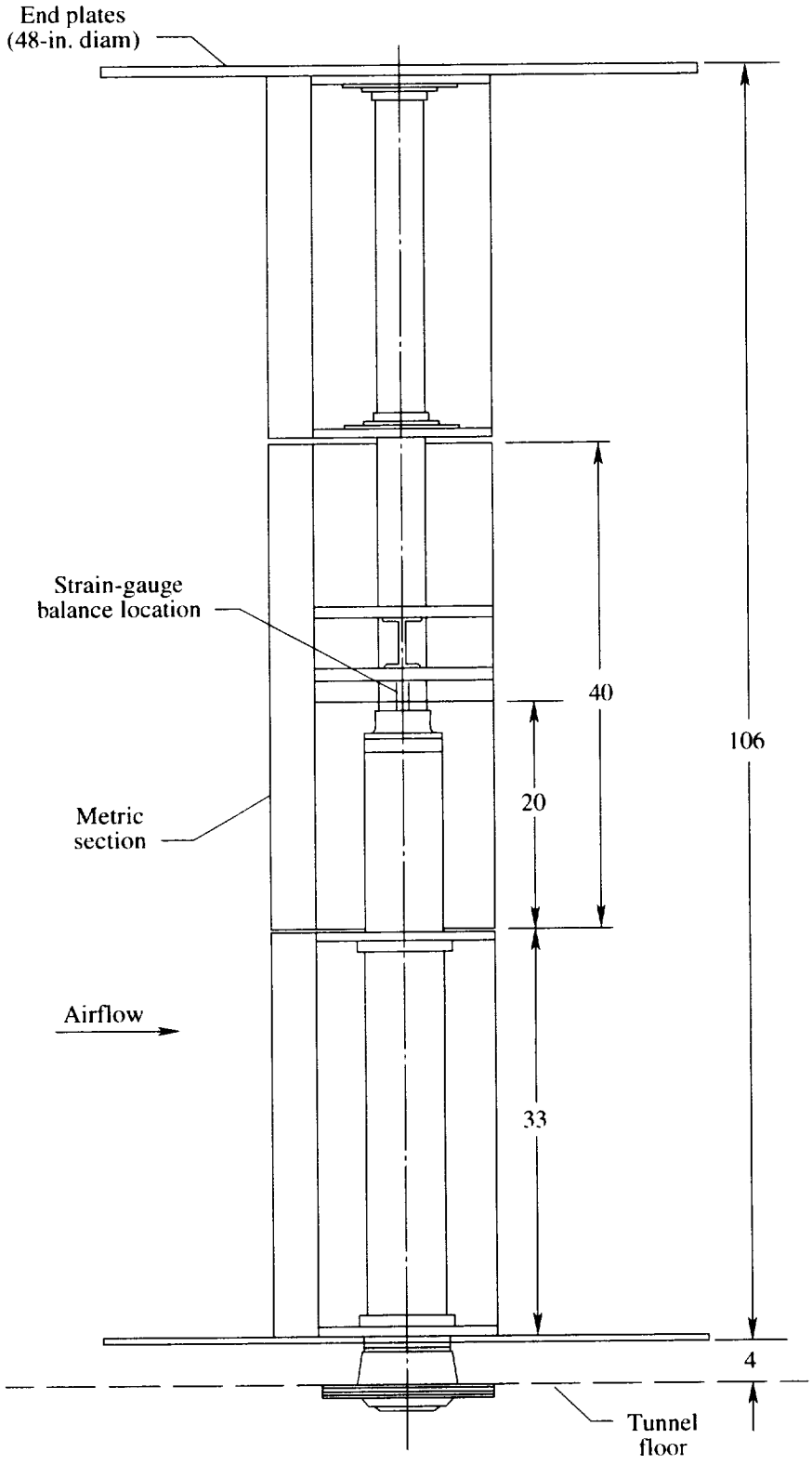

(a) Helicopter two-dimensional test apparatus; linear dimensions are in inches.

Figure 3. Sketch of model test apparatus and photographs taken in test section of Langley 14- by 22-Foot Subsonic Tunnel.

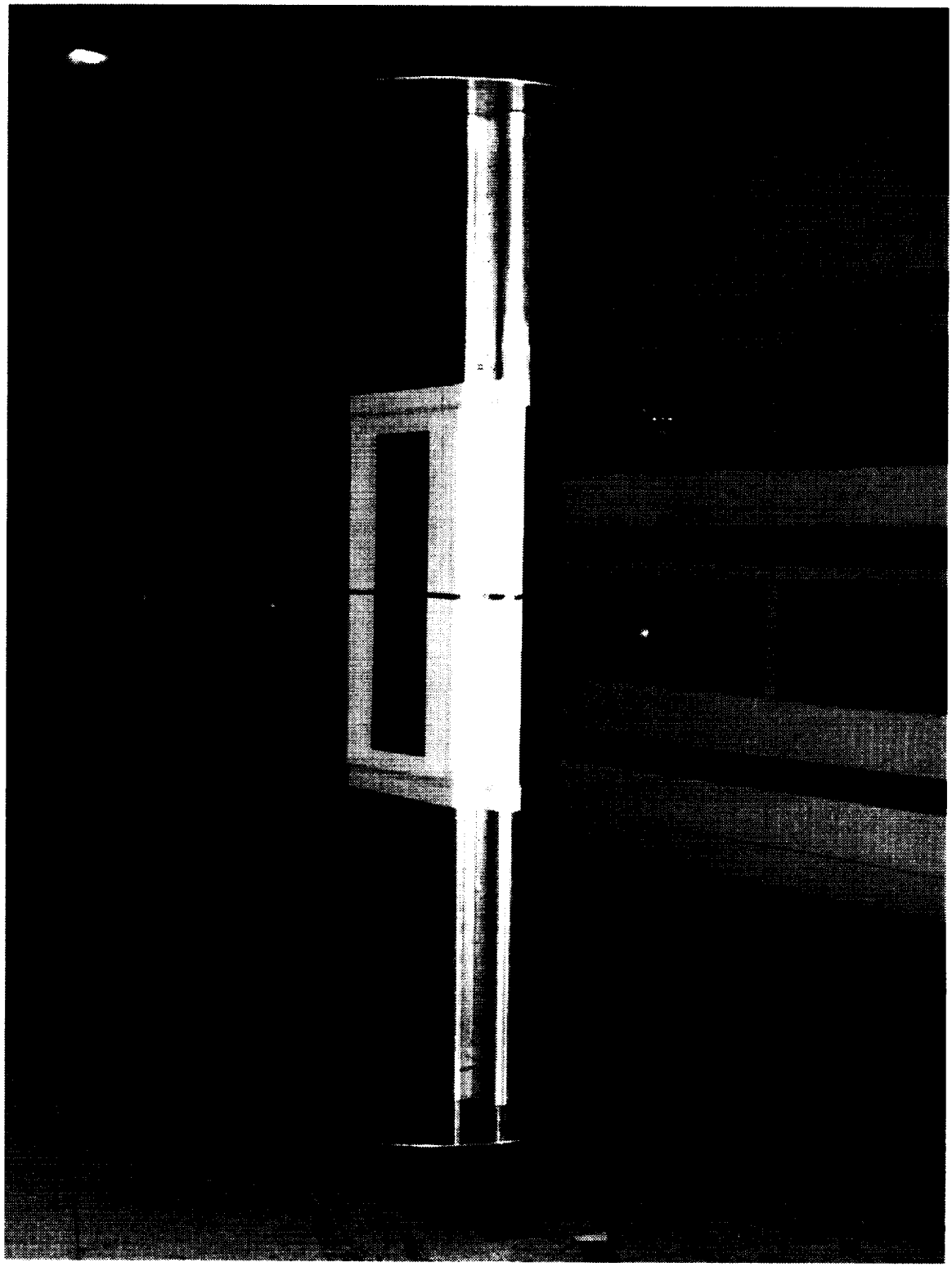

(b) Two-dimensional test apparatus in tunnel.

Figure 3. Continued.

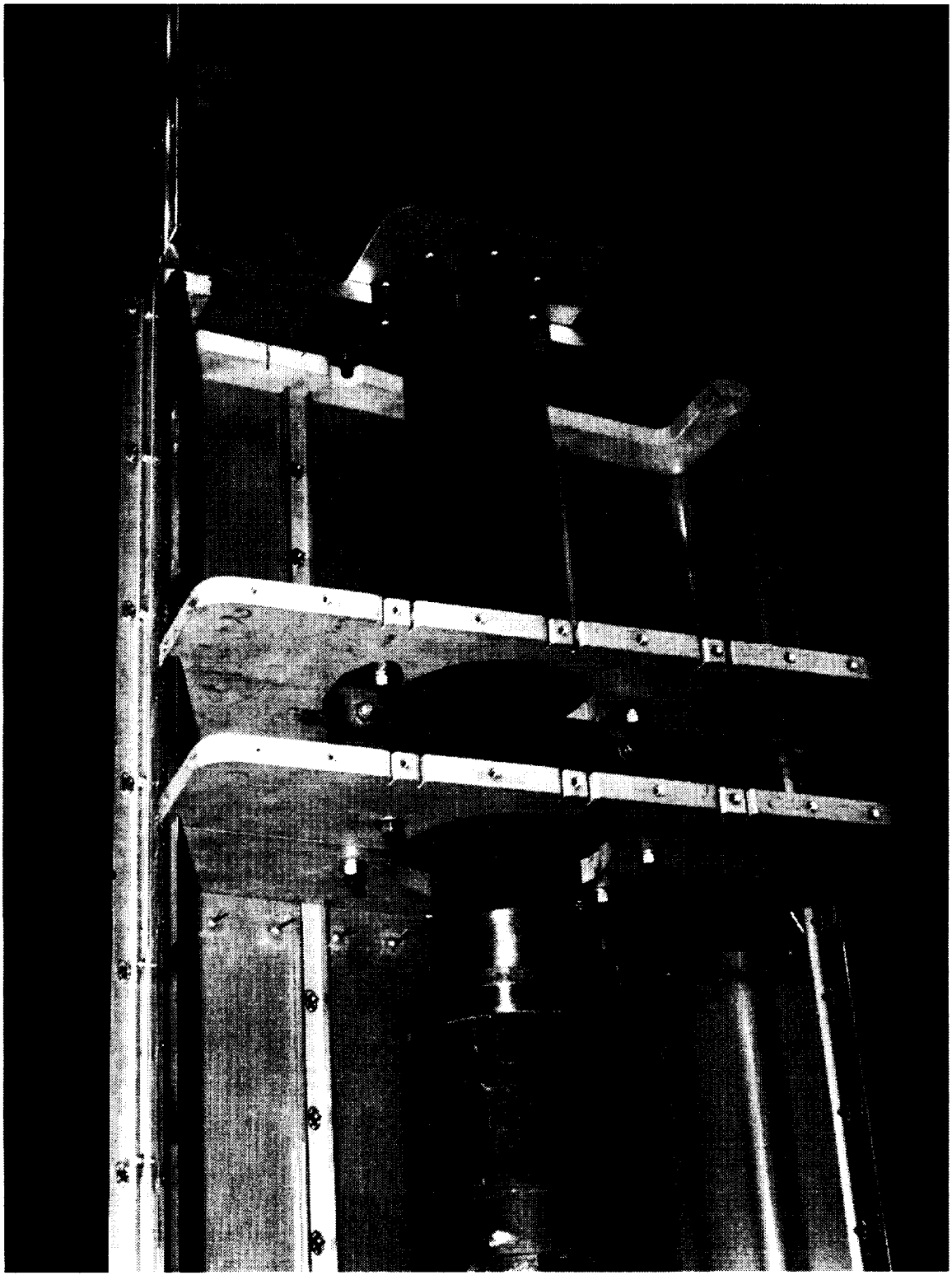

(c) Photograph showing internal construction of metric section of model.

Figure 3. Concluded.

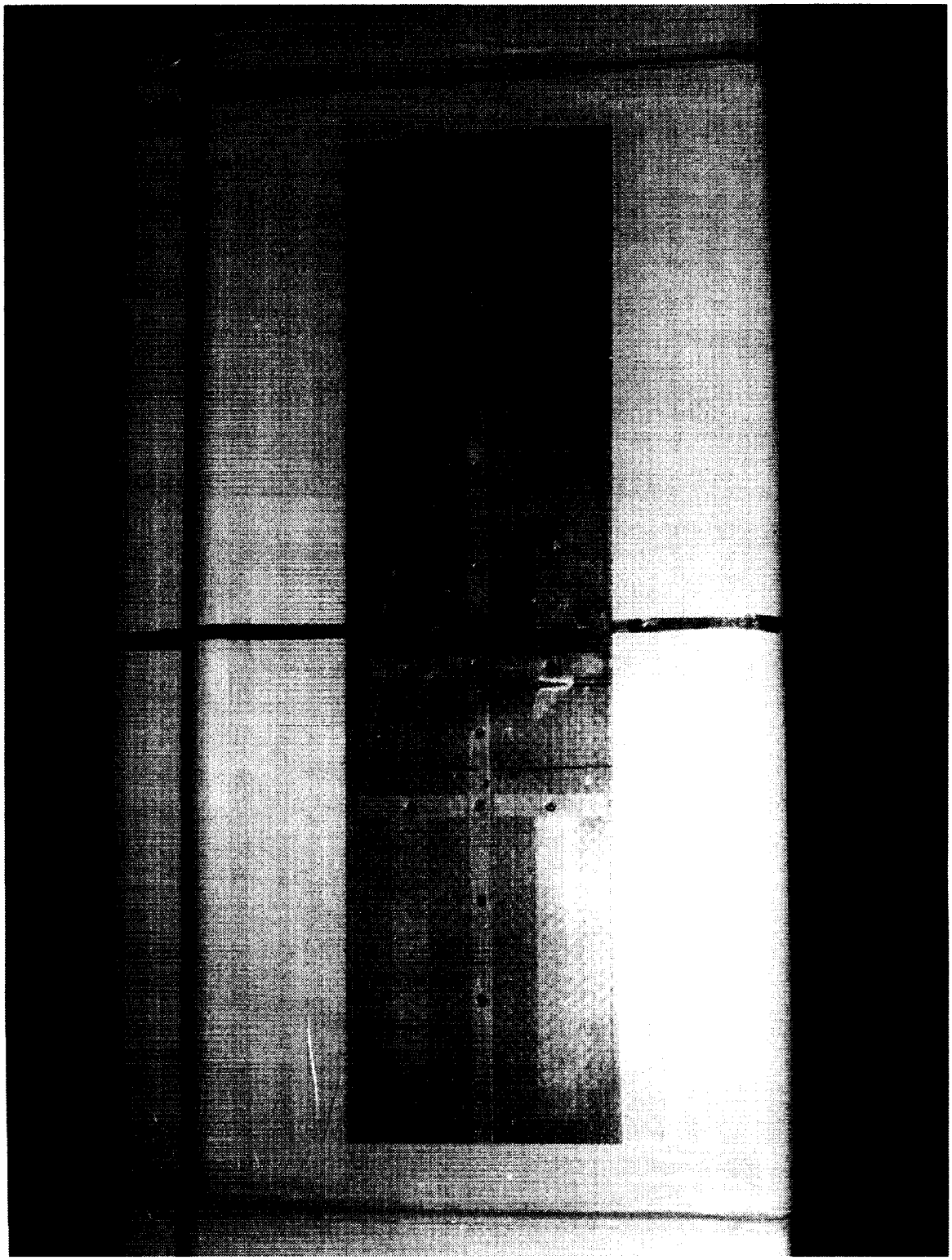

Figure 4. Close-up of metric section of model in tunnel showing example of use of tape to vary vented area.

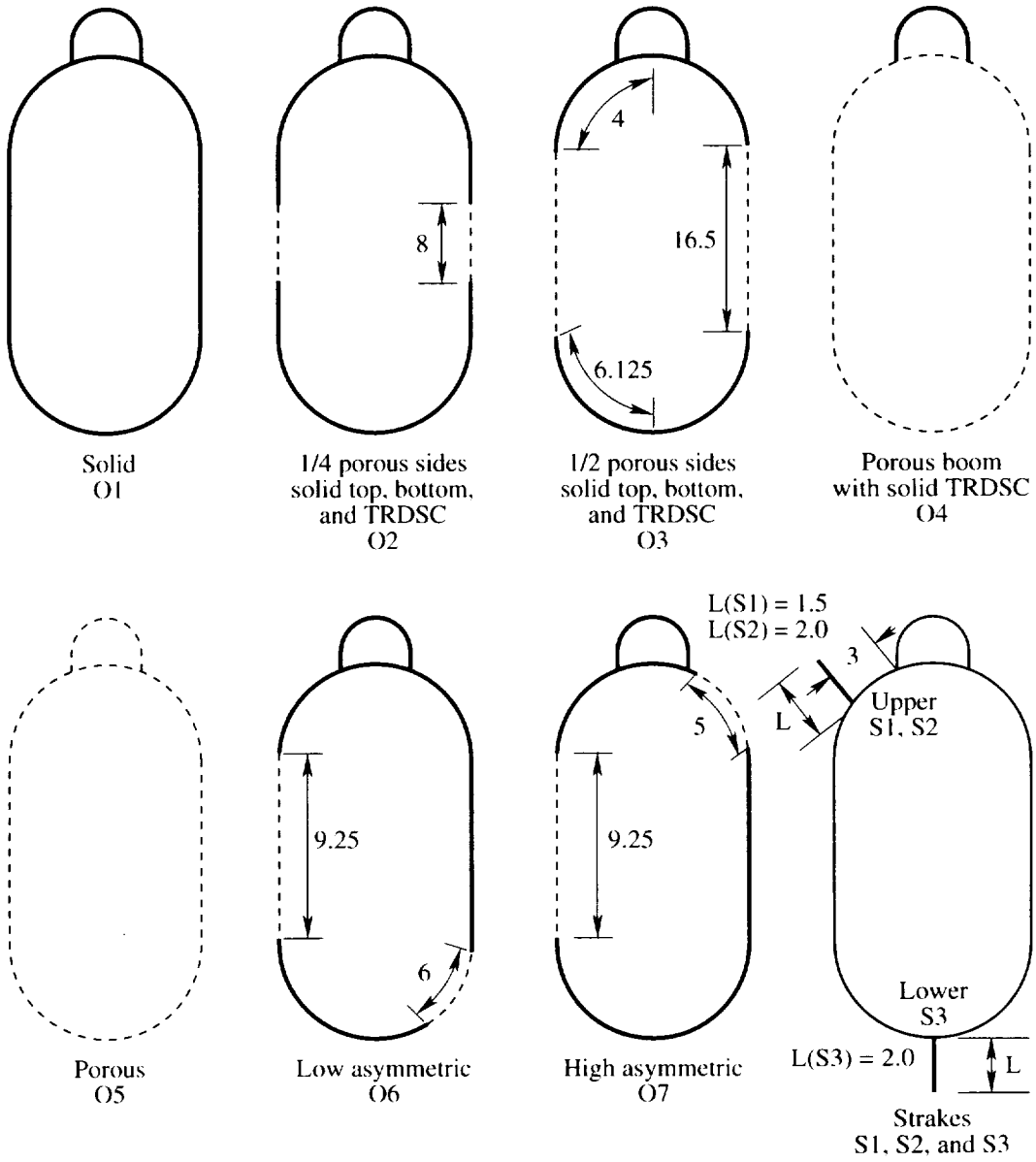

(a) Oval boom configurations.

Figure 5. Configuration definition. Dashed lines denote vented areas; linear dimensions are in inches.

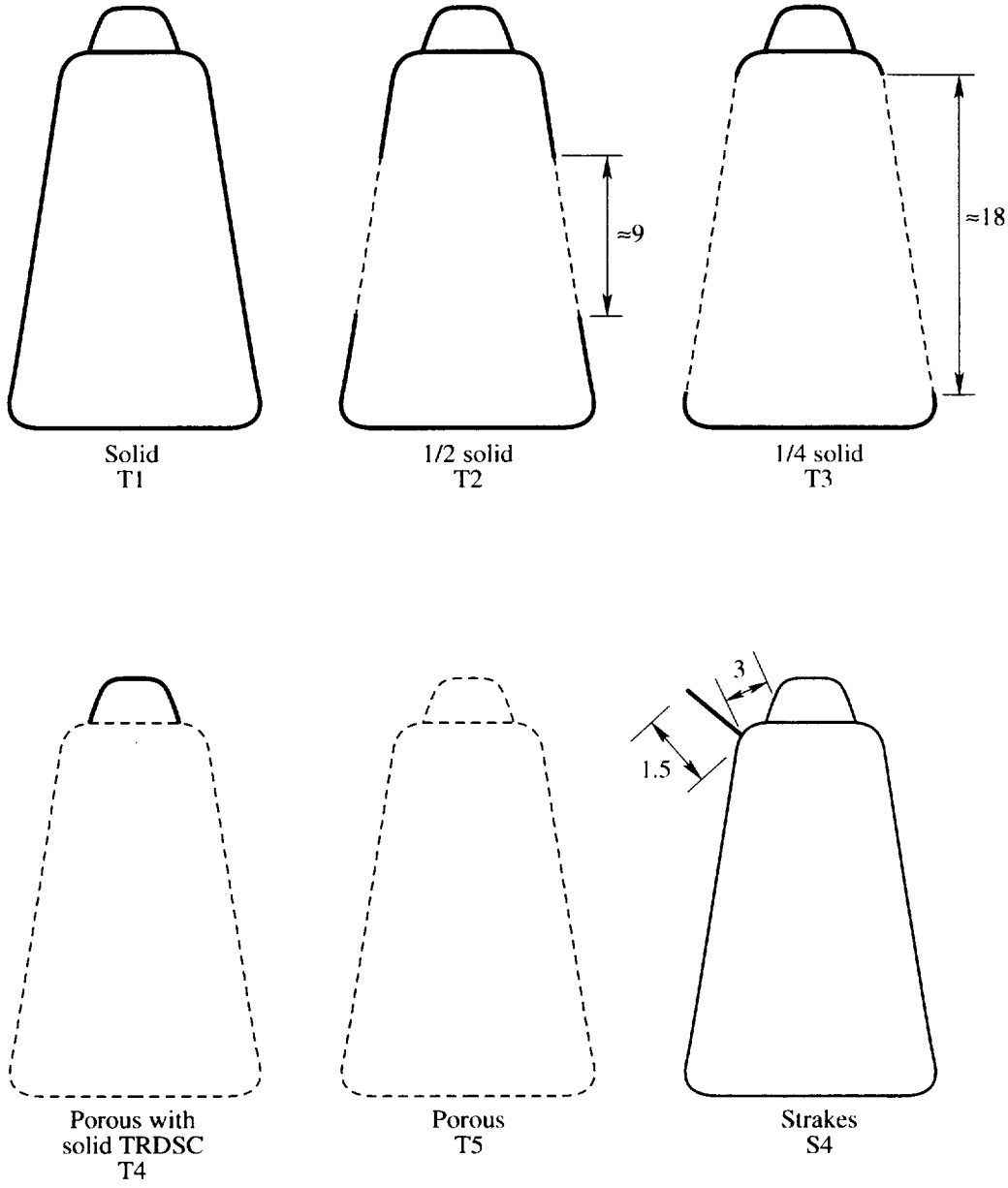

(b) Trapezoidal boom configurations.

Figure 5. Concluded.

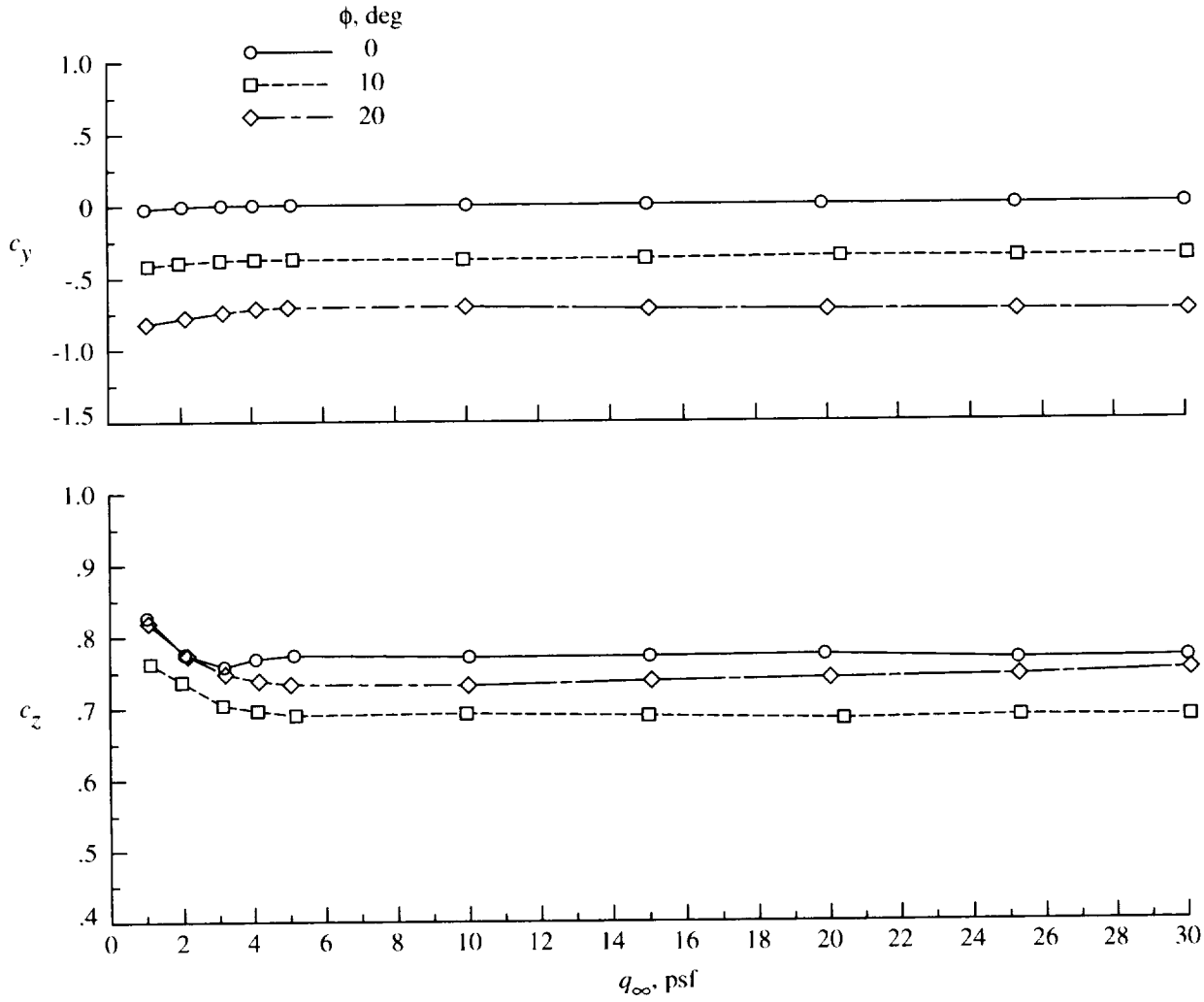

(a) $\phi = 0°$, 10°, and 20°.

Figure 6. Normal and side force characteristics of oval boom shape with full porosity.

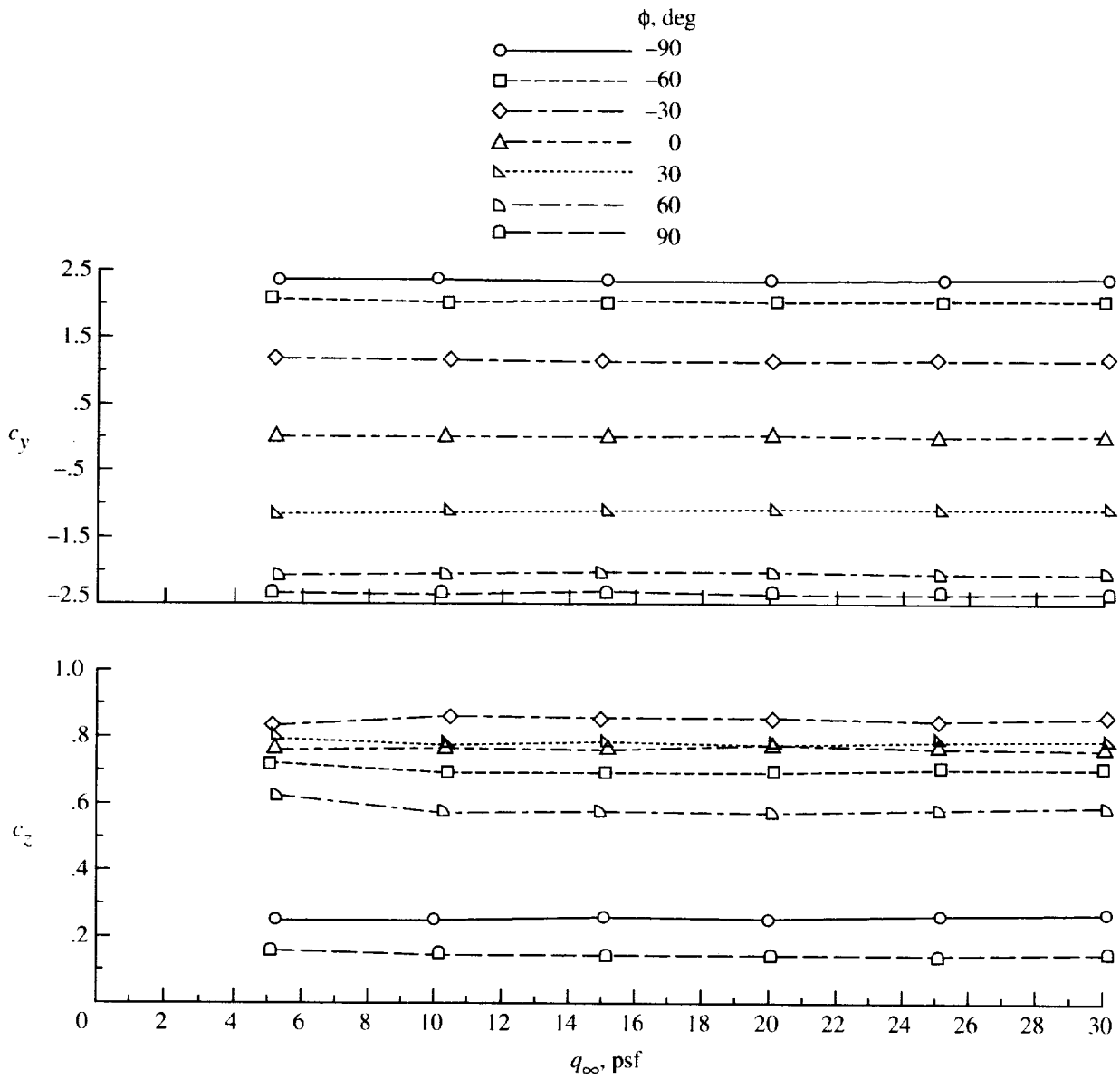

(b) $\phi = \pm 30°$, $\pm 60°$, and $\pm 90°$.

Figure 6. Continued.

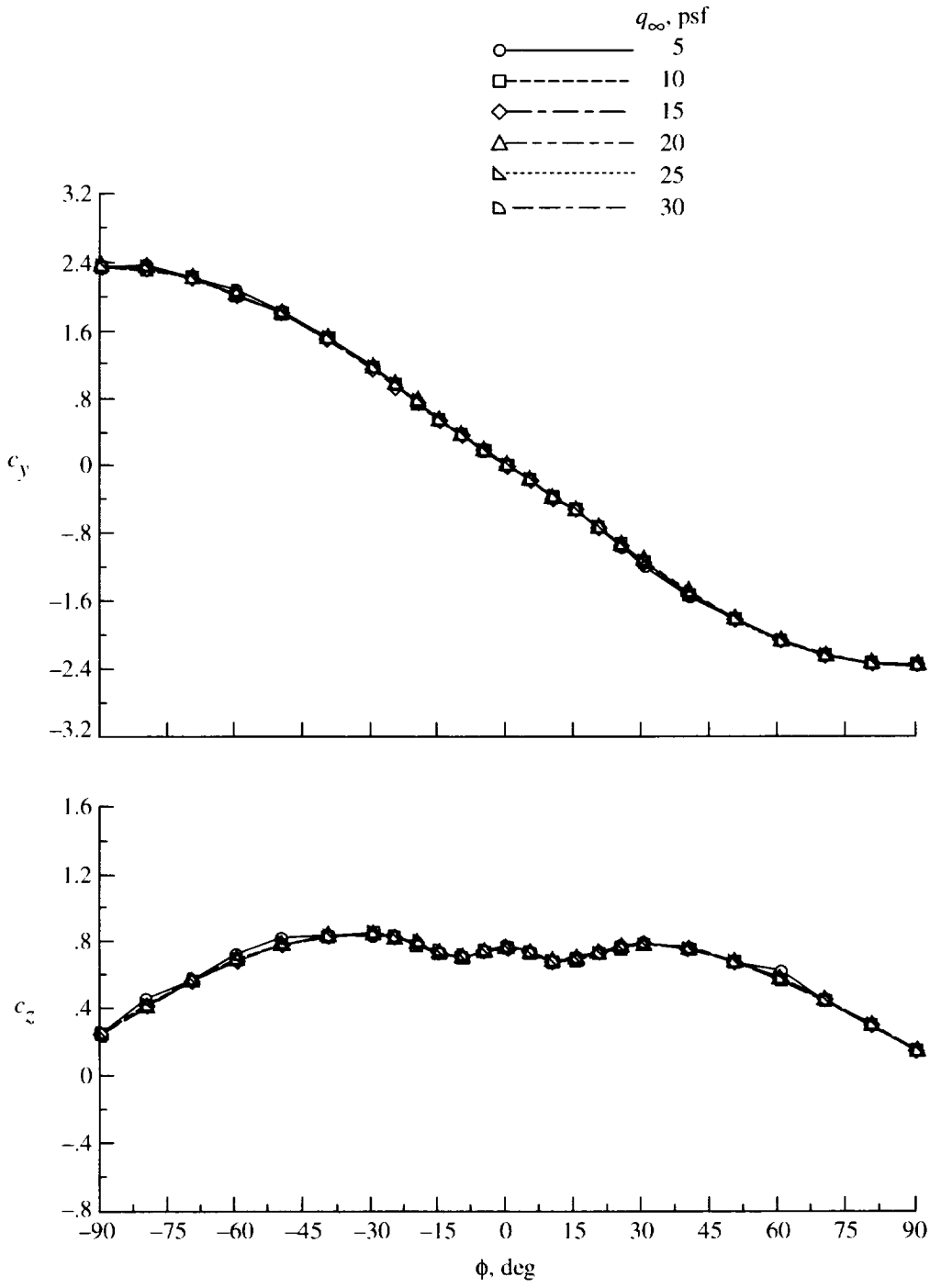

(c) Dynamic pressure.

Figure 6. Concluded.

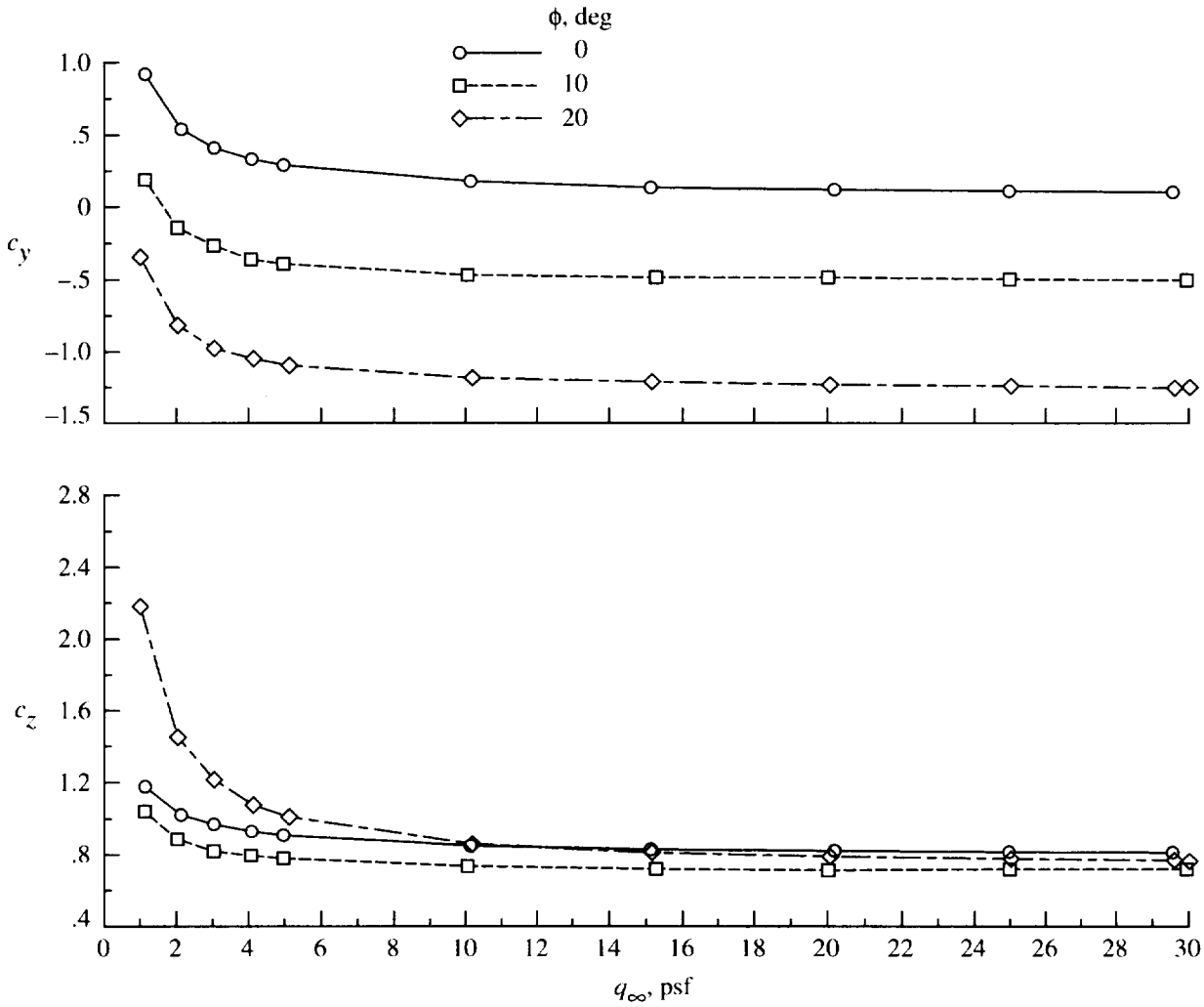

(a) $\phi = 0°$, 10°, and 20°.

Figure 7. Normal and side force characteristics of trapezoidal boom shape with full porosity.

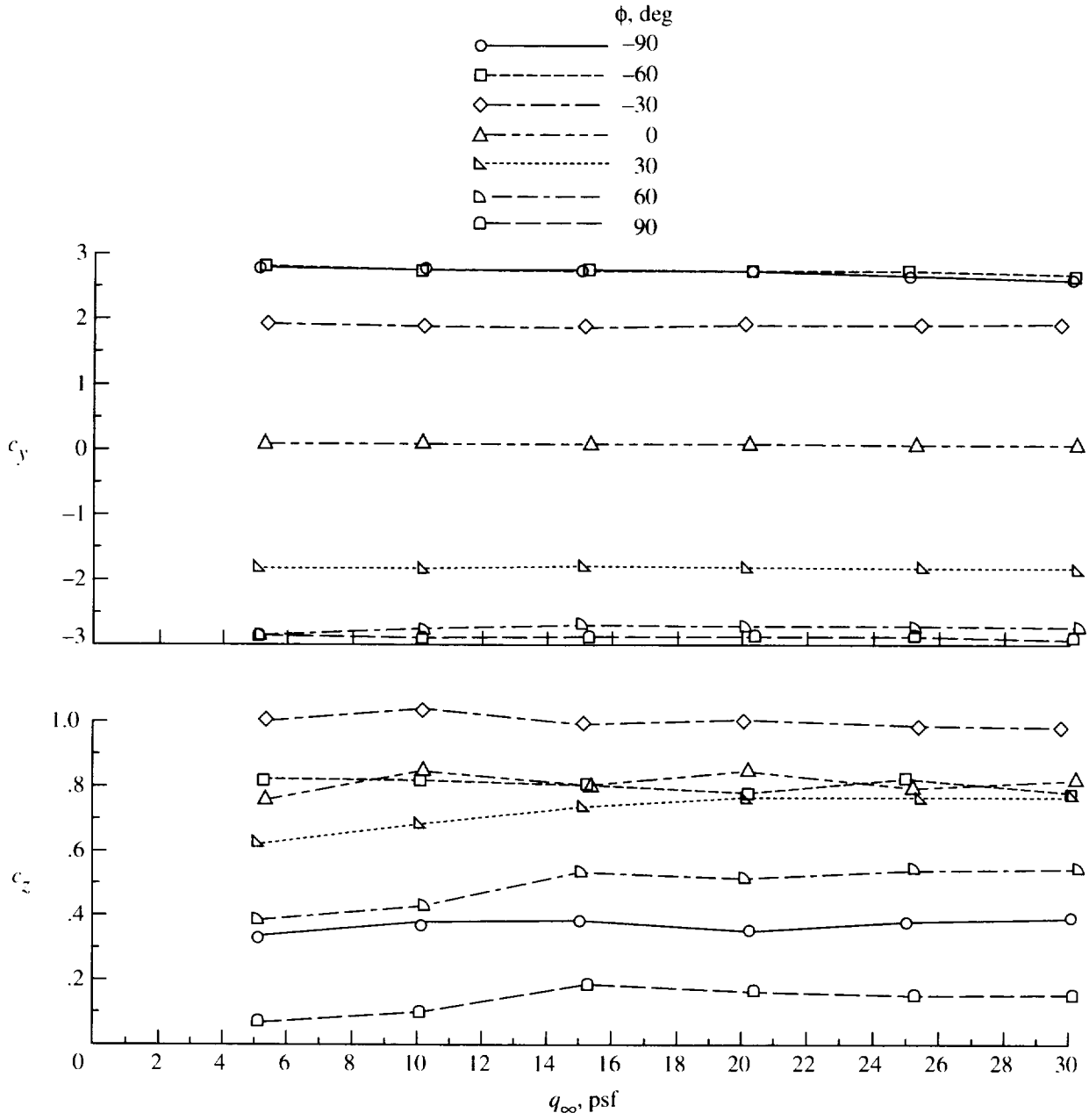

(b) $\phi = \pm 30°$, $\pm 60°$, and $\pm 90°$.

Figure 7. Continued.

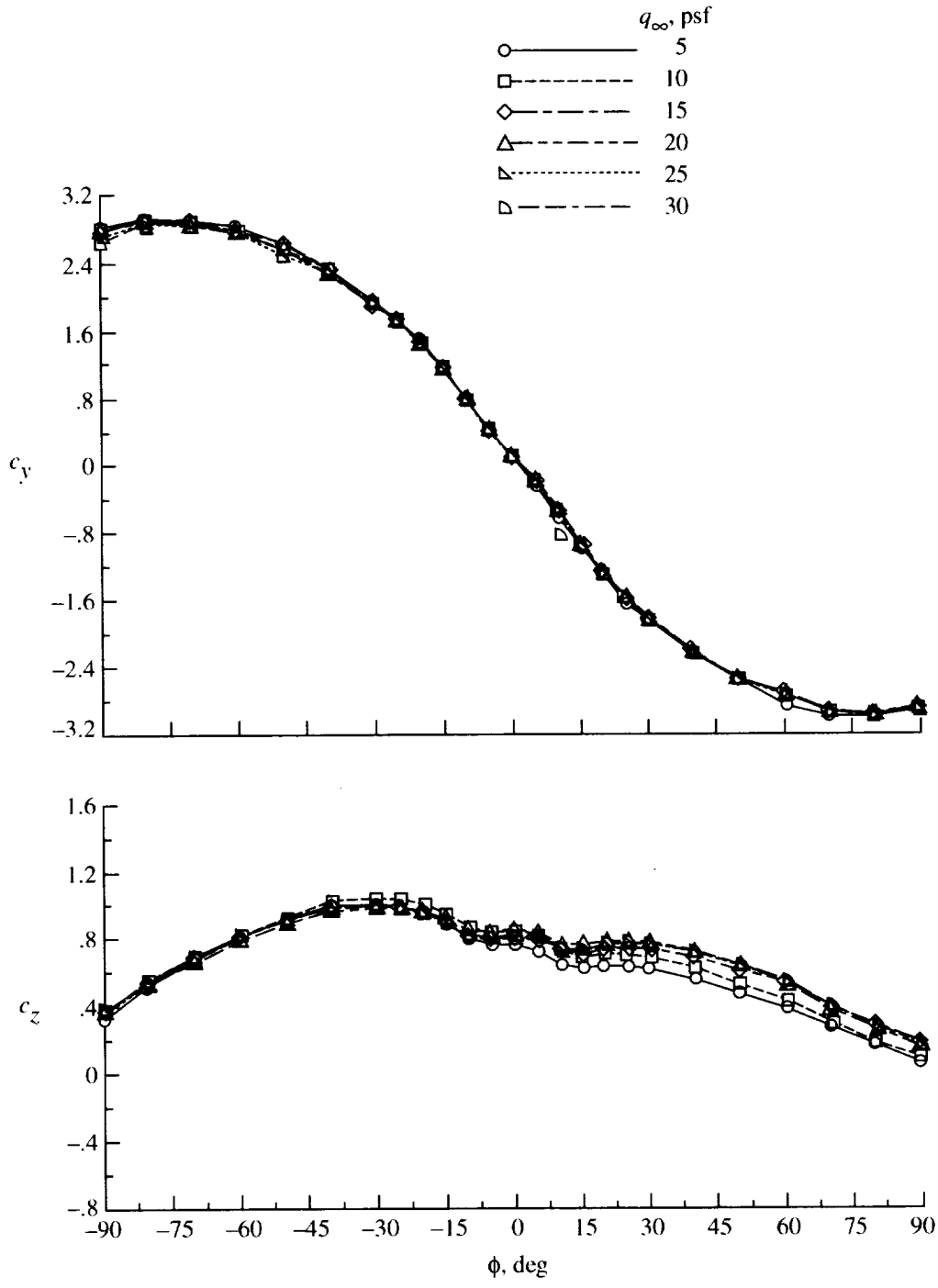

(c) Dynamic pressure.

Figure 7. Concluded.

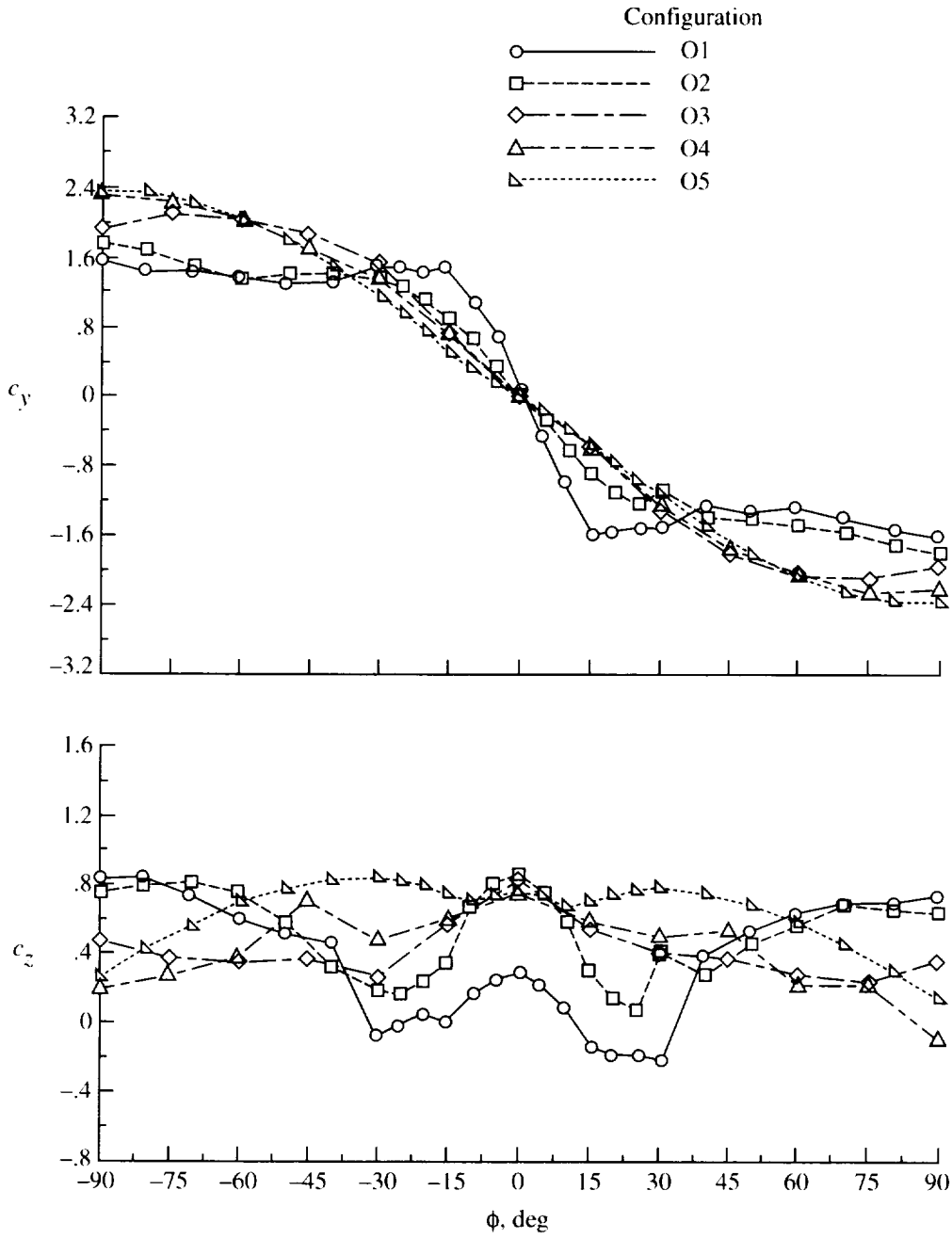

(a) q_∞ = 20 and 25 psf.

Figure 8. Effect of venting configuration on oval tail boom normal and side force coefficients for symmetric configurations.

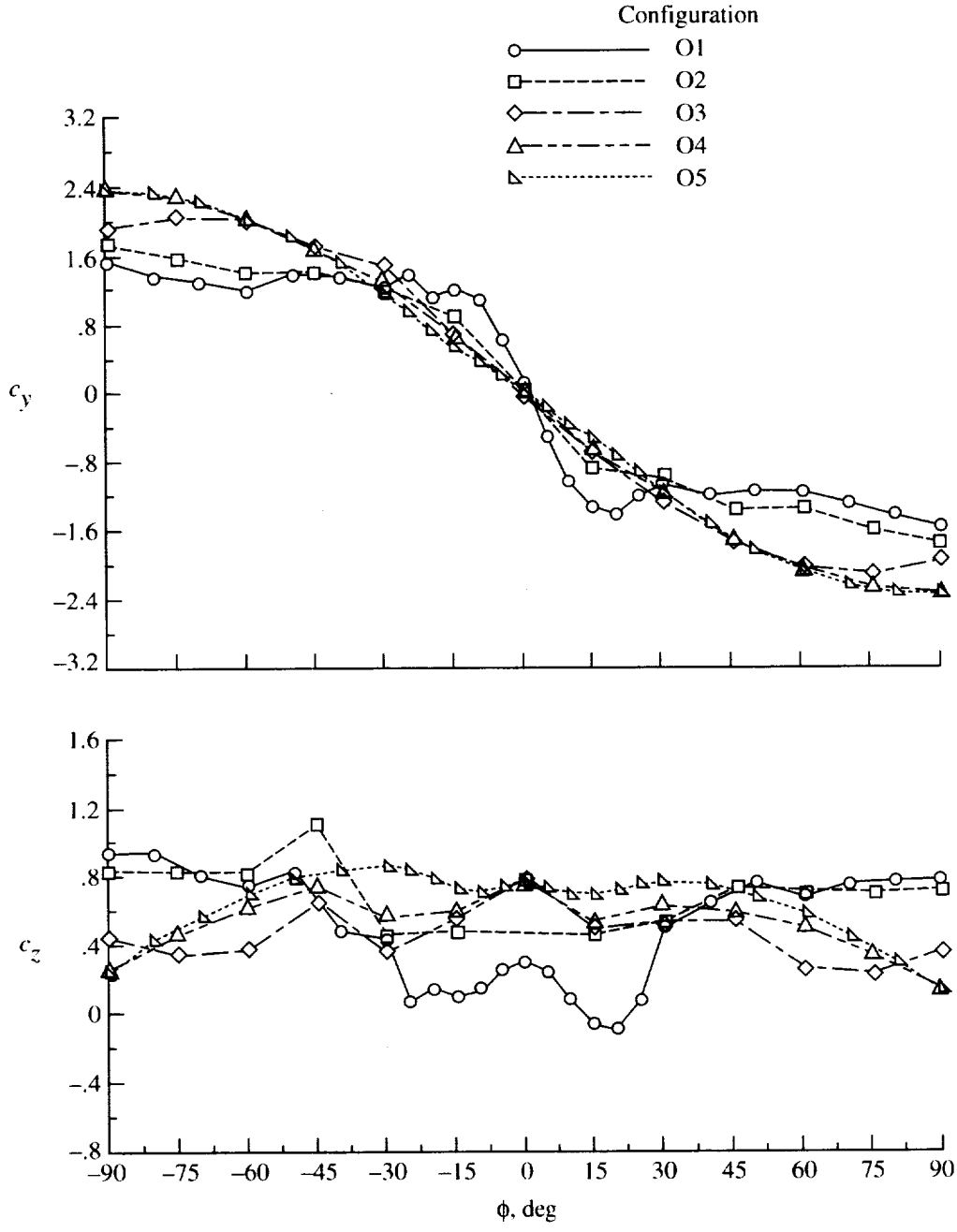

(b) q_∞ = 10 psf.

Figure 8. Concluded.

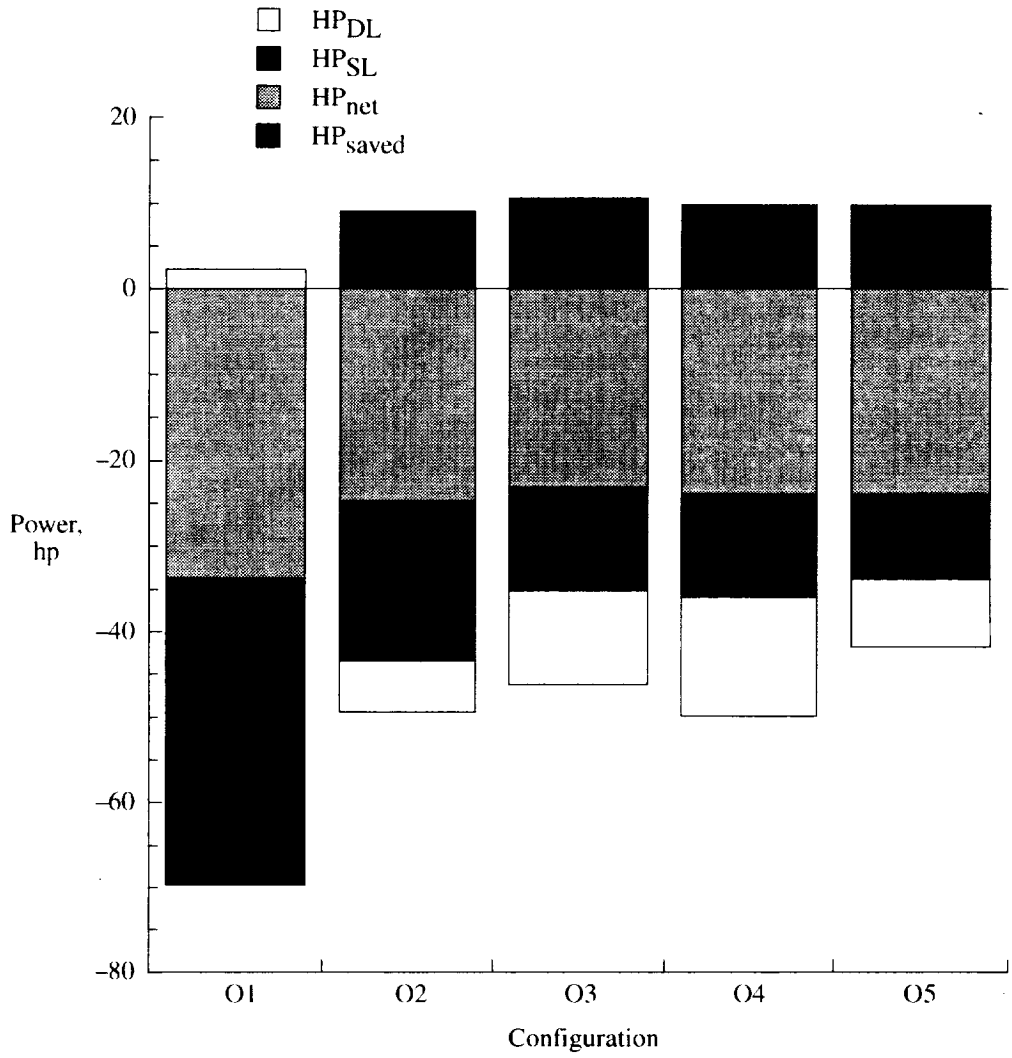

Figure 9. Calculated power required of helicopter with various tail boom configurations, oval cross section.

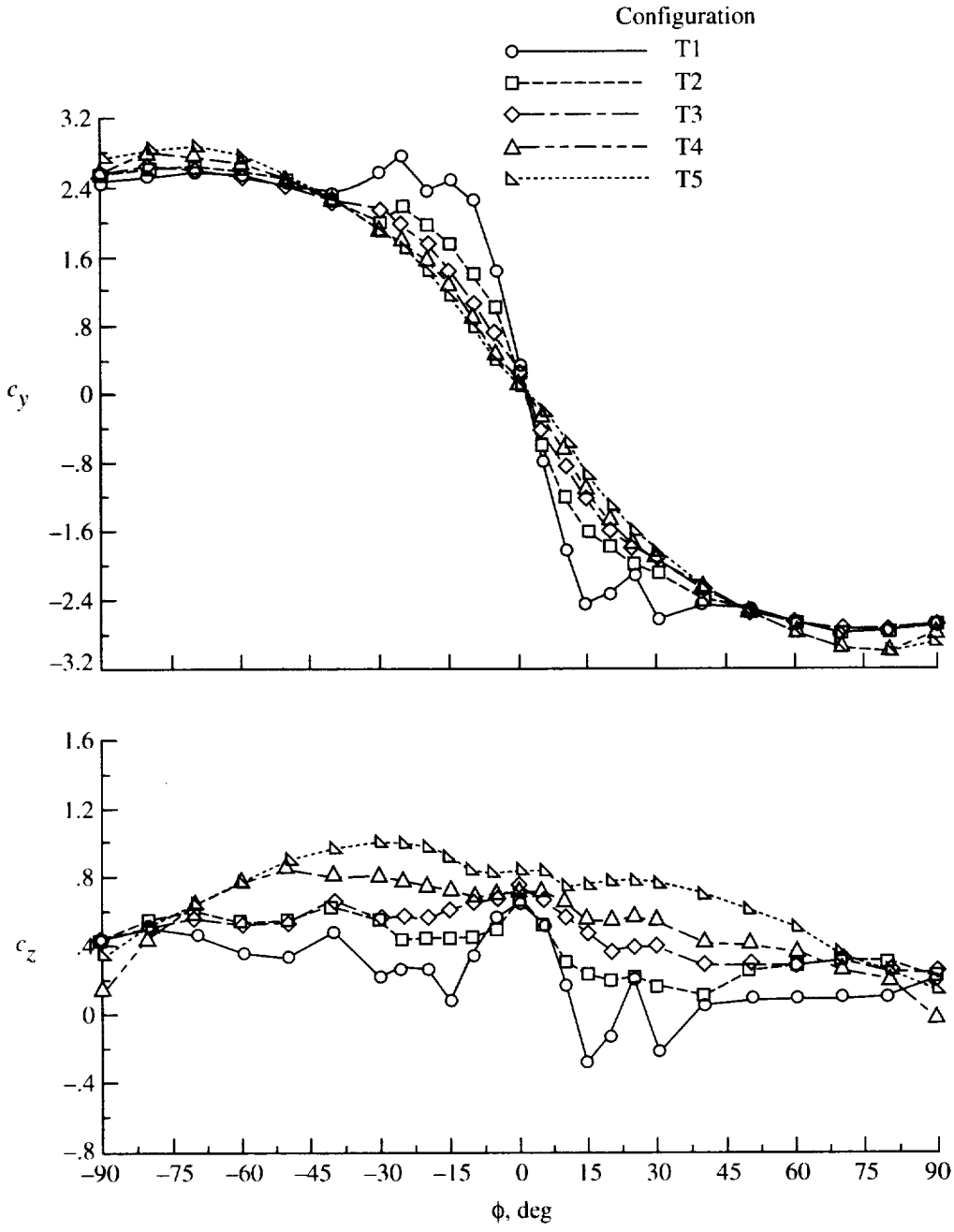

Figure 10. Effect of venting configuration on trapezoidal tail boom normal and side force coefficients for q_∞ = 20 and 25 psf.

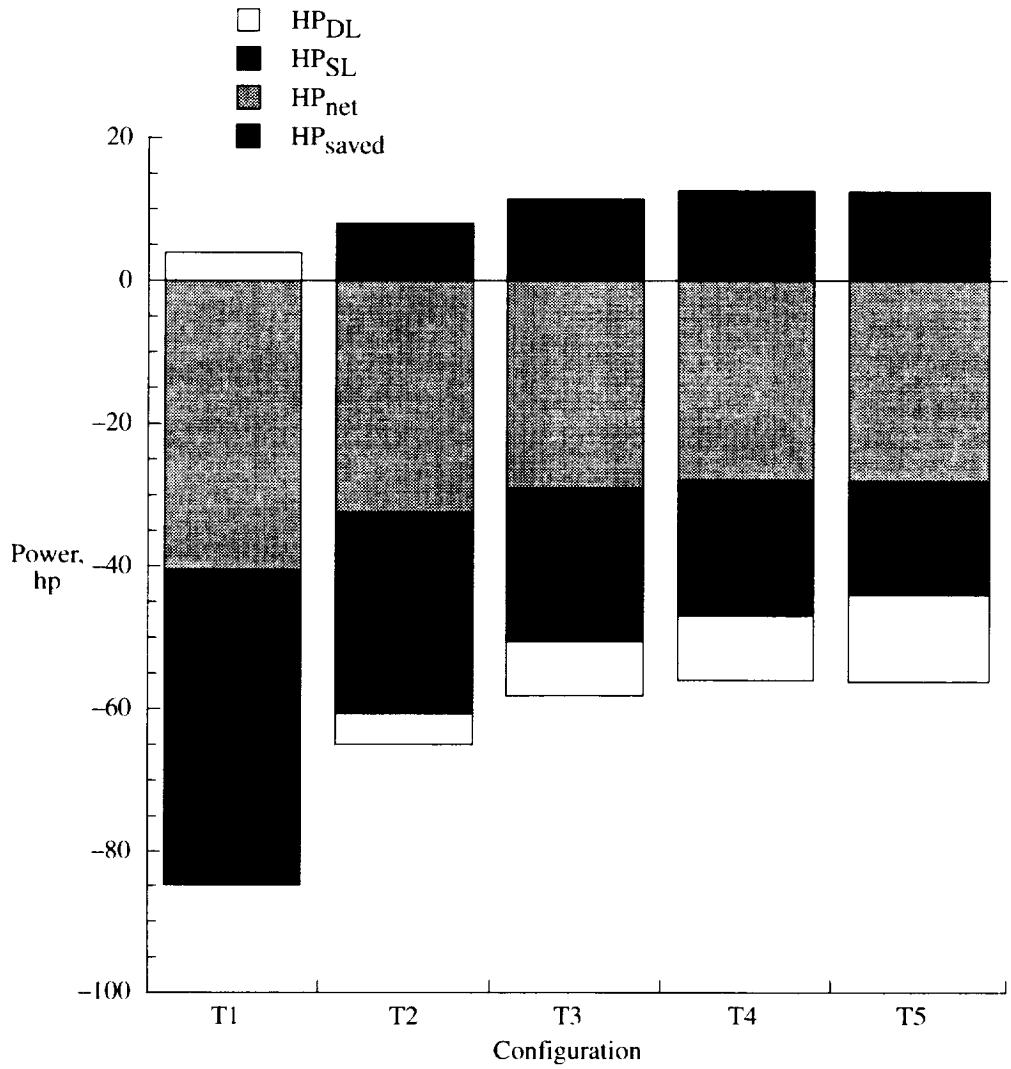

Figure 11. Calculated power required of helicopter with various tail boom configurations, trapezoidal cross section.

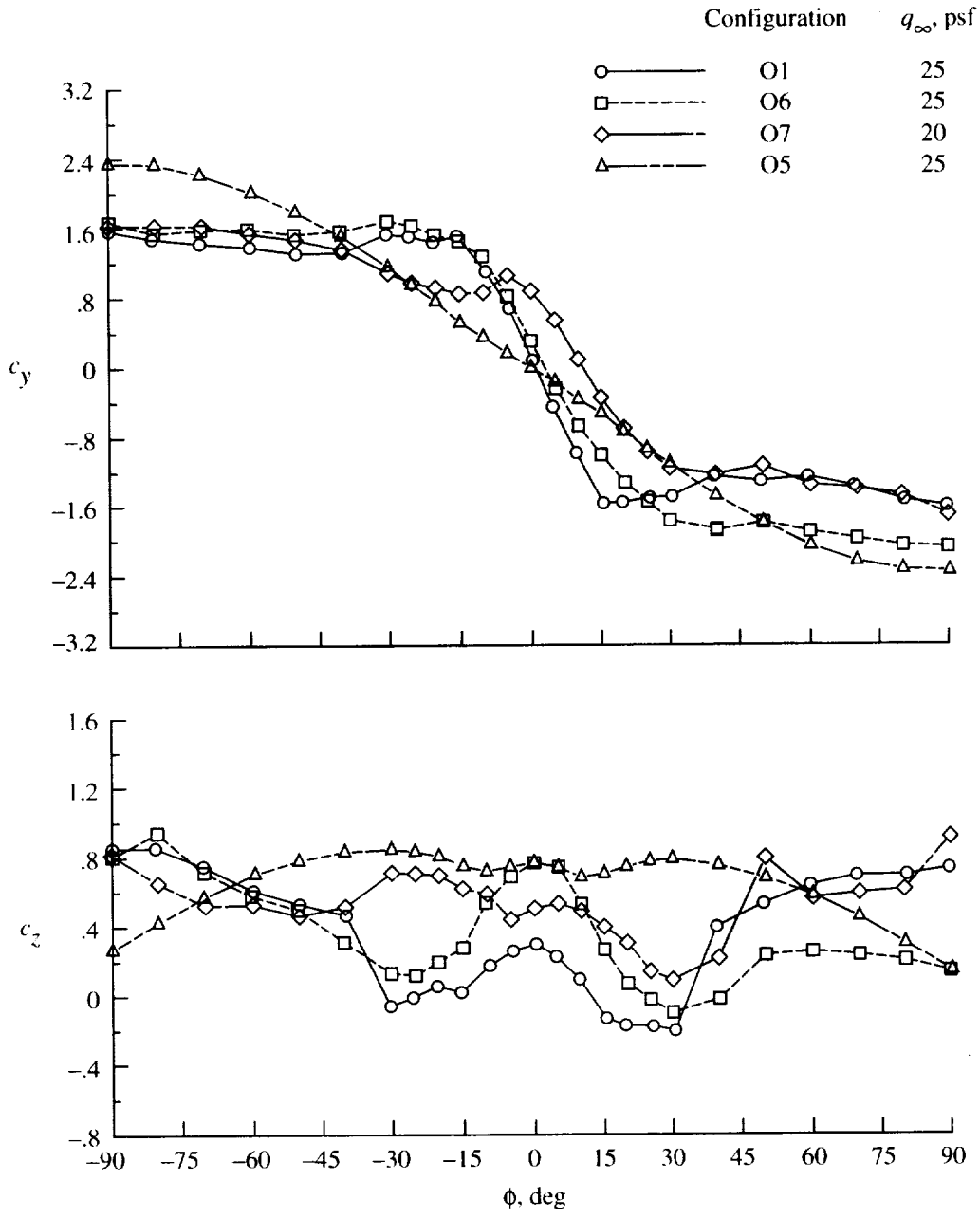

(a) q_∞ = 20 and 25 psf.

Figure 12. Effect of venting configuration on oval tail boom normal and side force coefficients for asymmetric configurations.

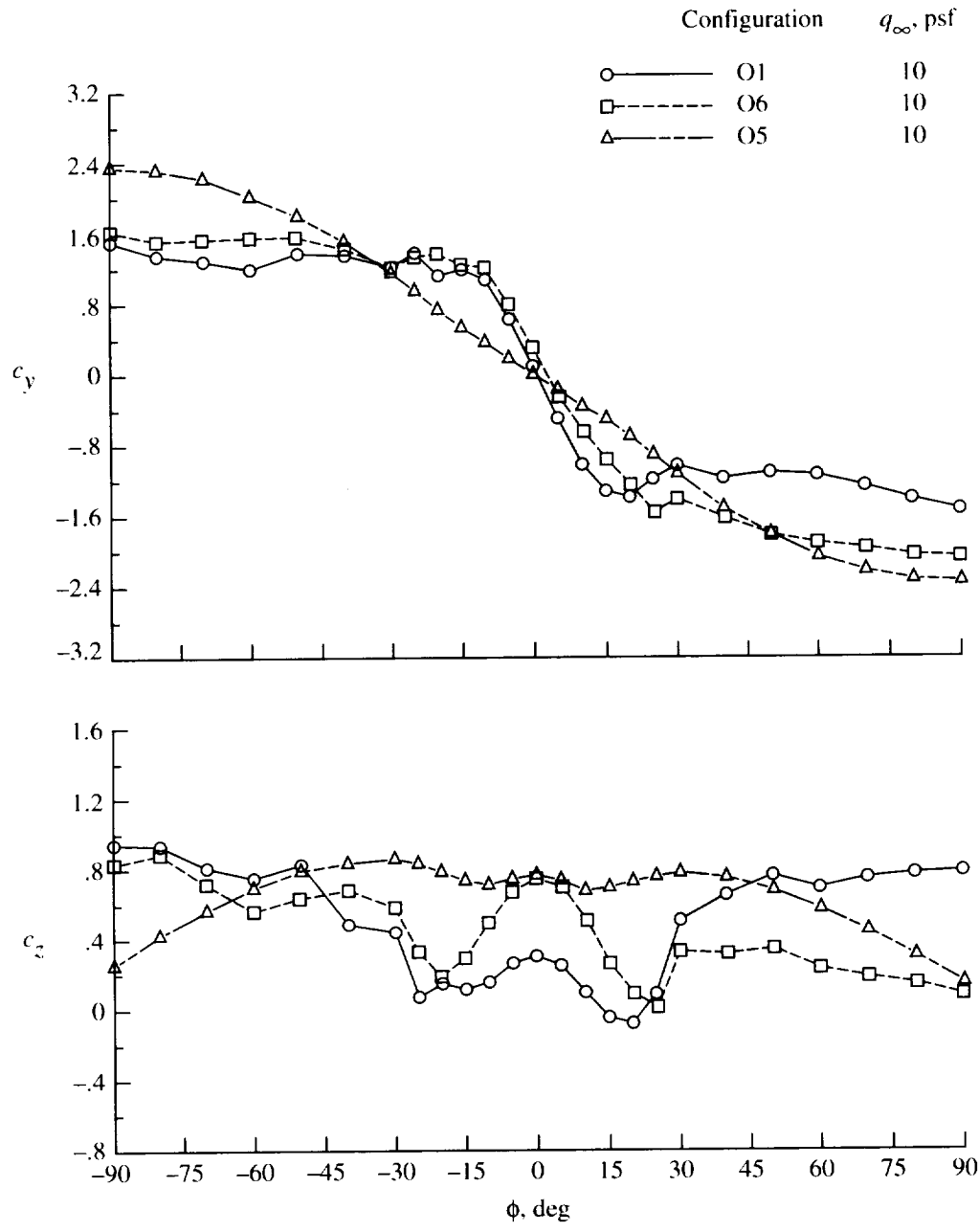

(b) q_∞ = 10 psf.

Figure 12. Concluded.

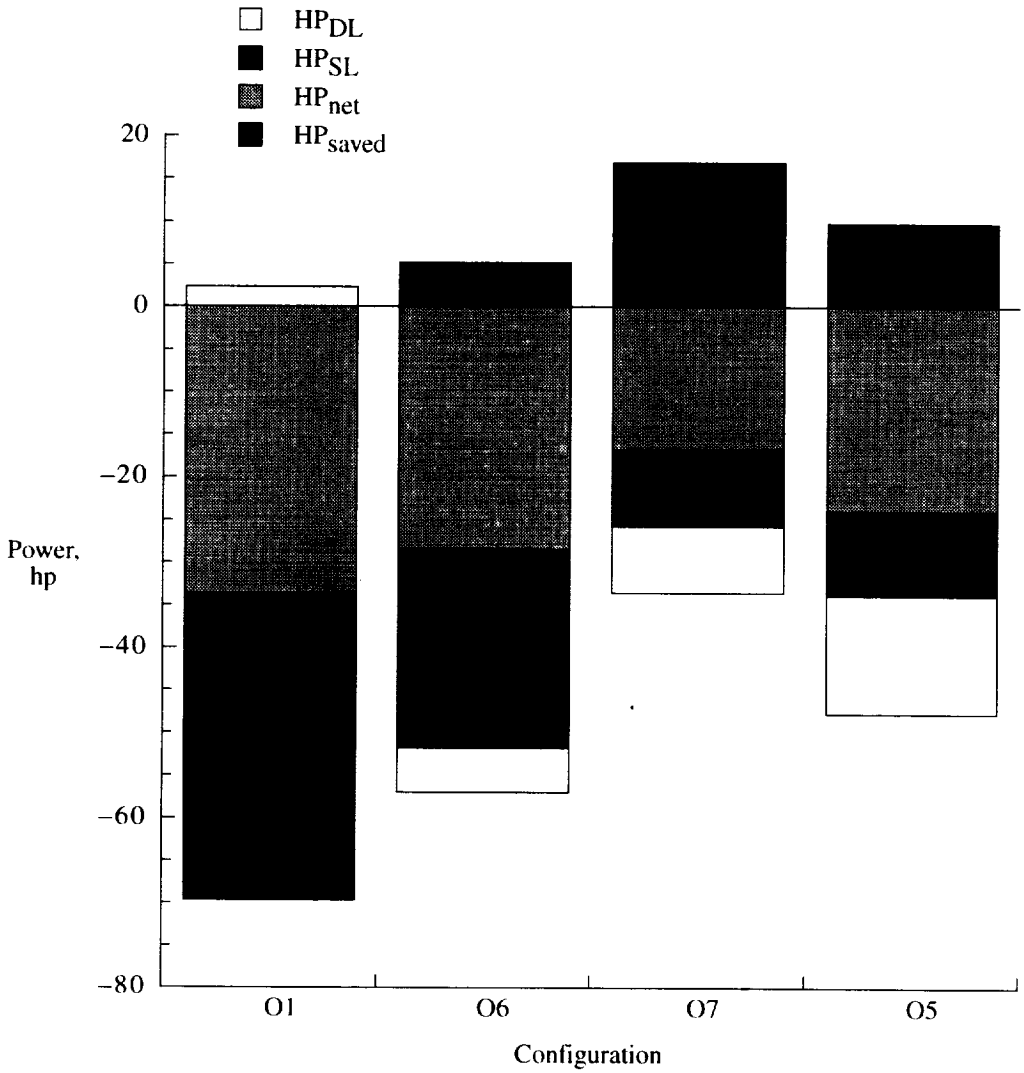

Figure 13. Calculated power required of helicopter with various tail boom configurations, oval cross section, asymmetric venting.

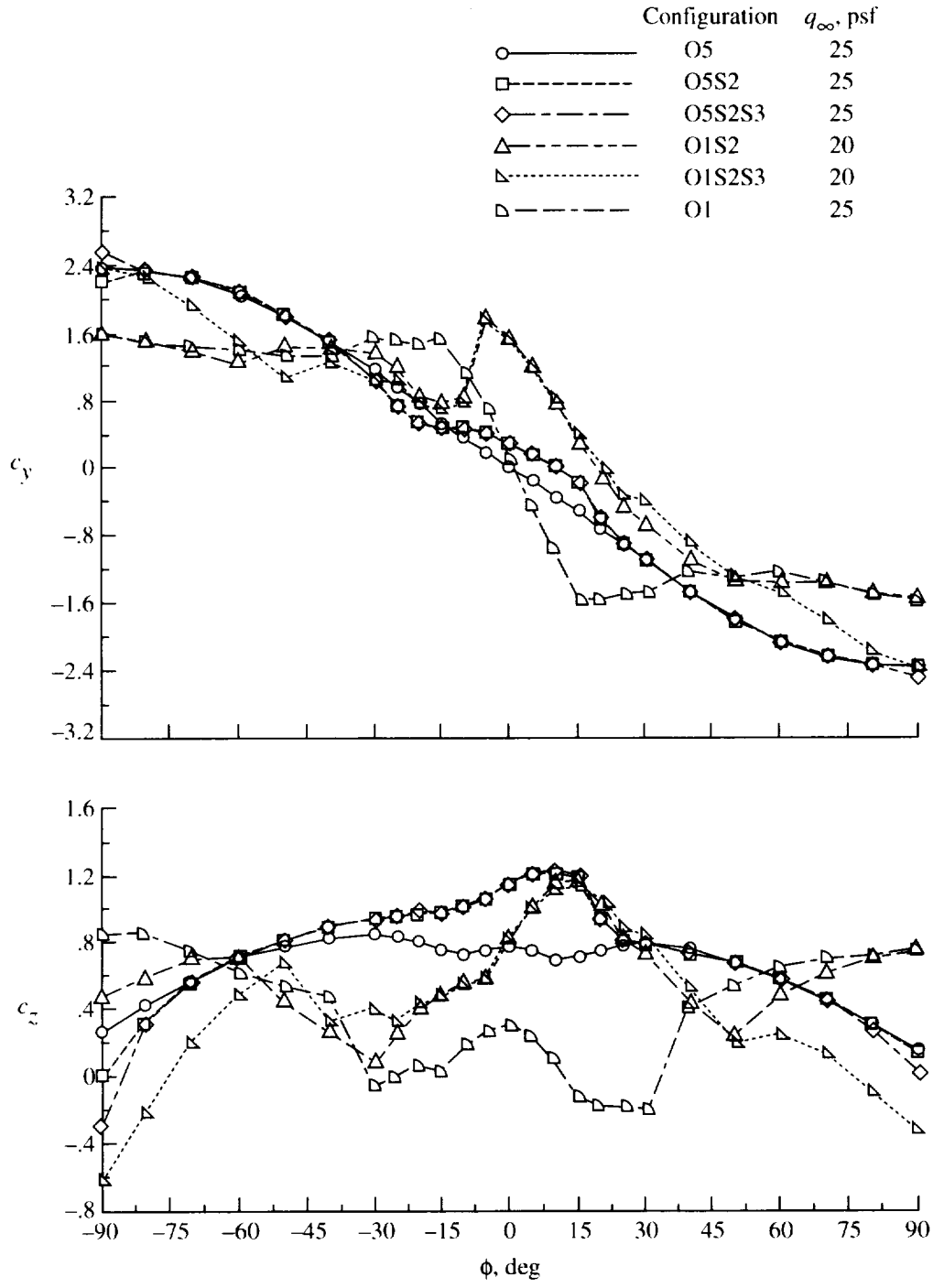

(a) q_∞ = 20 and 25 psf.

Figure 14. Effect of venting configuration and strakes on oval tail boom normal and side force coefficients.

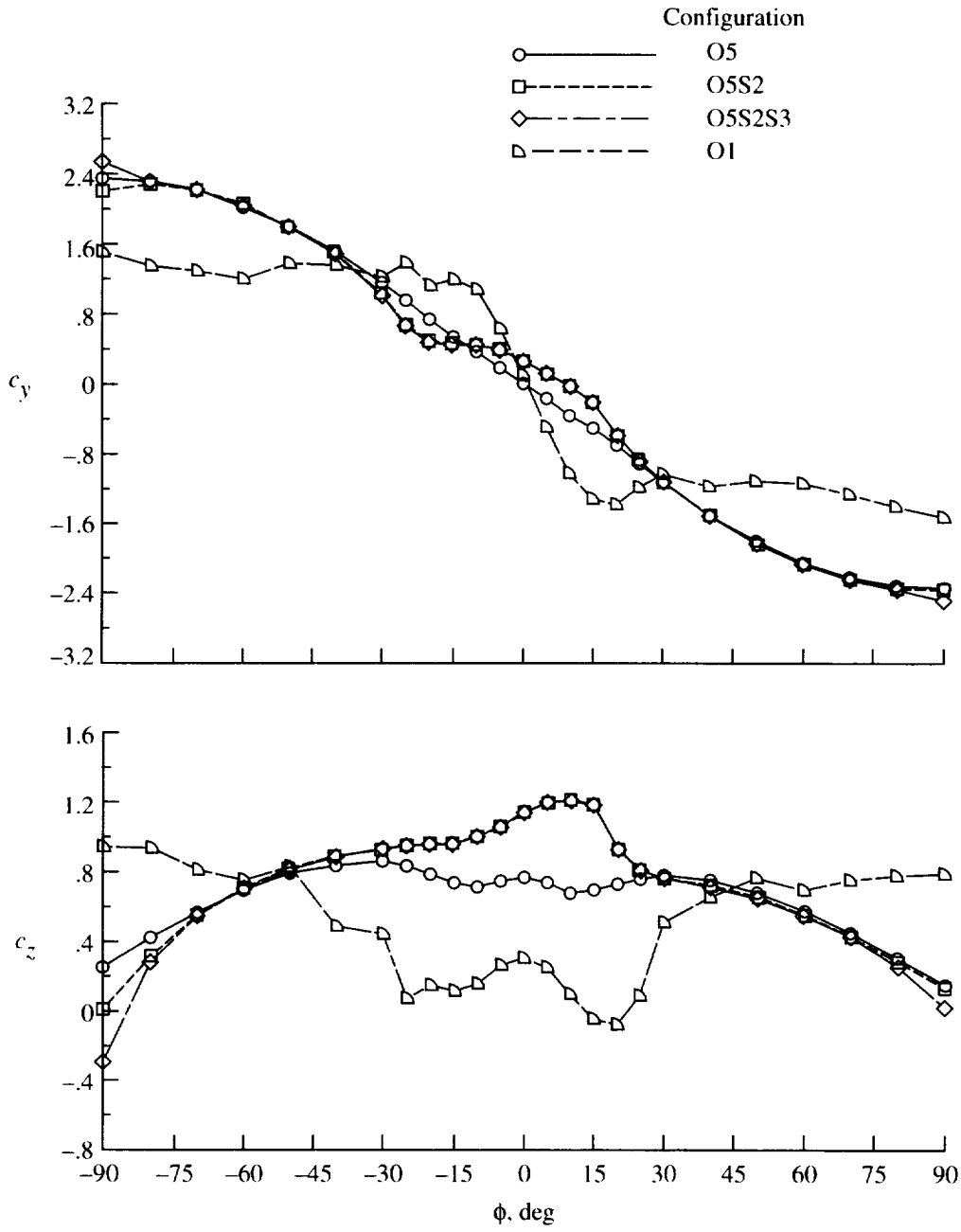

(b) q_∞ = 10 psf.

Figure 14. Concluded.

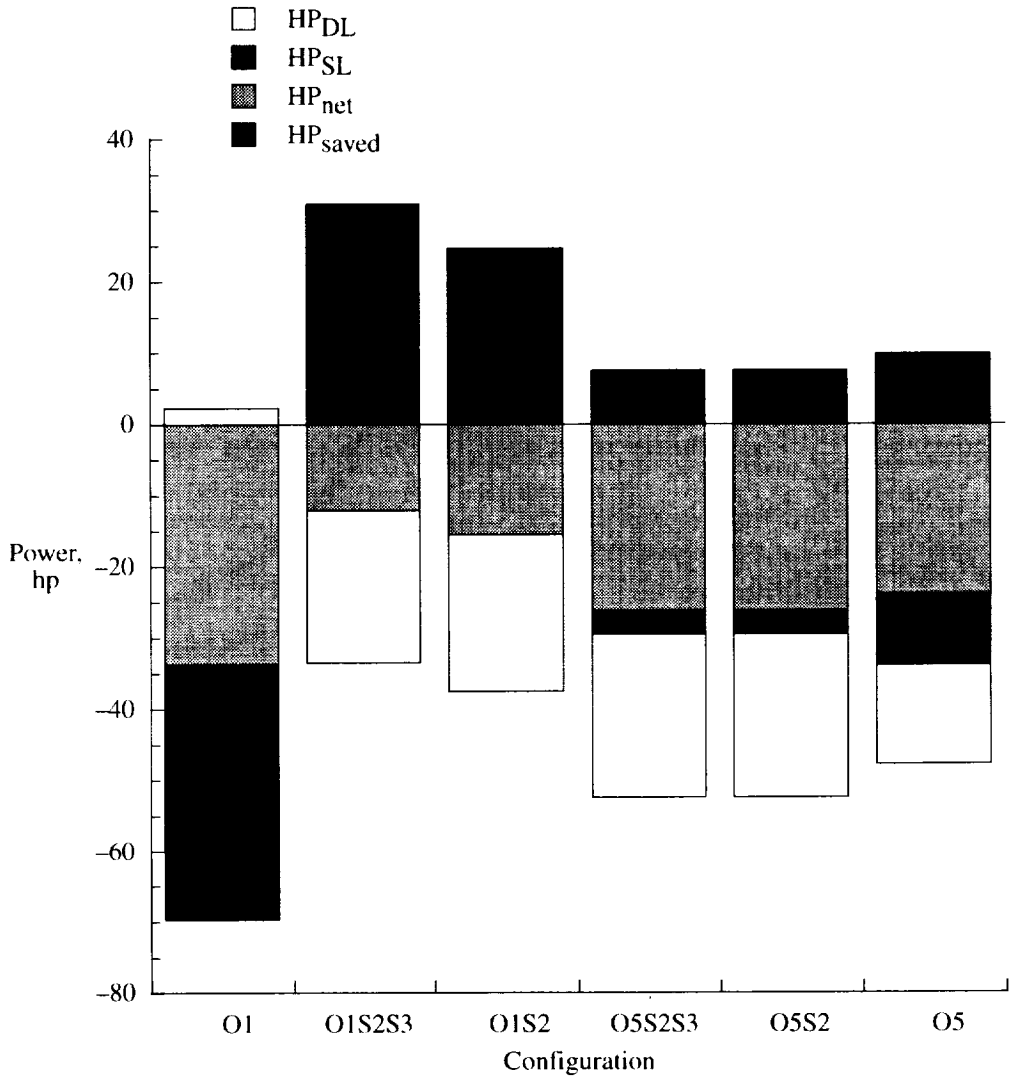

Figure 15. Calculated power required of helicopter with various tail boom configurations, oval cross section, boom strakes.

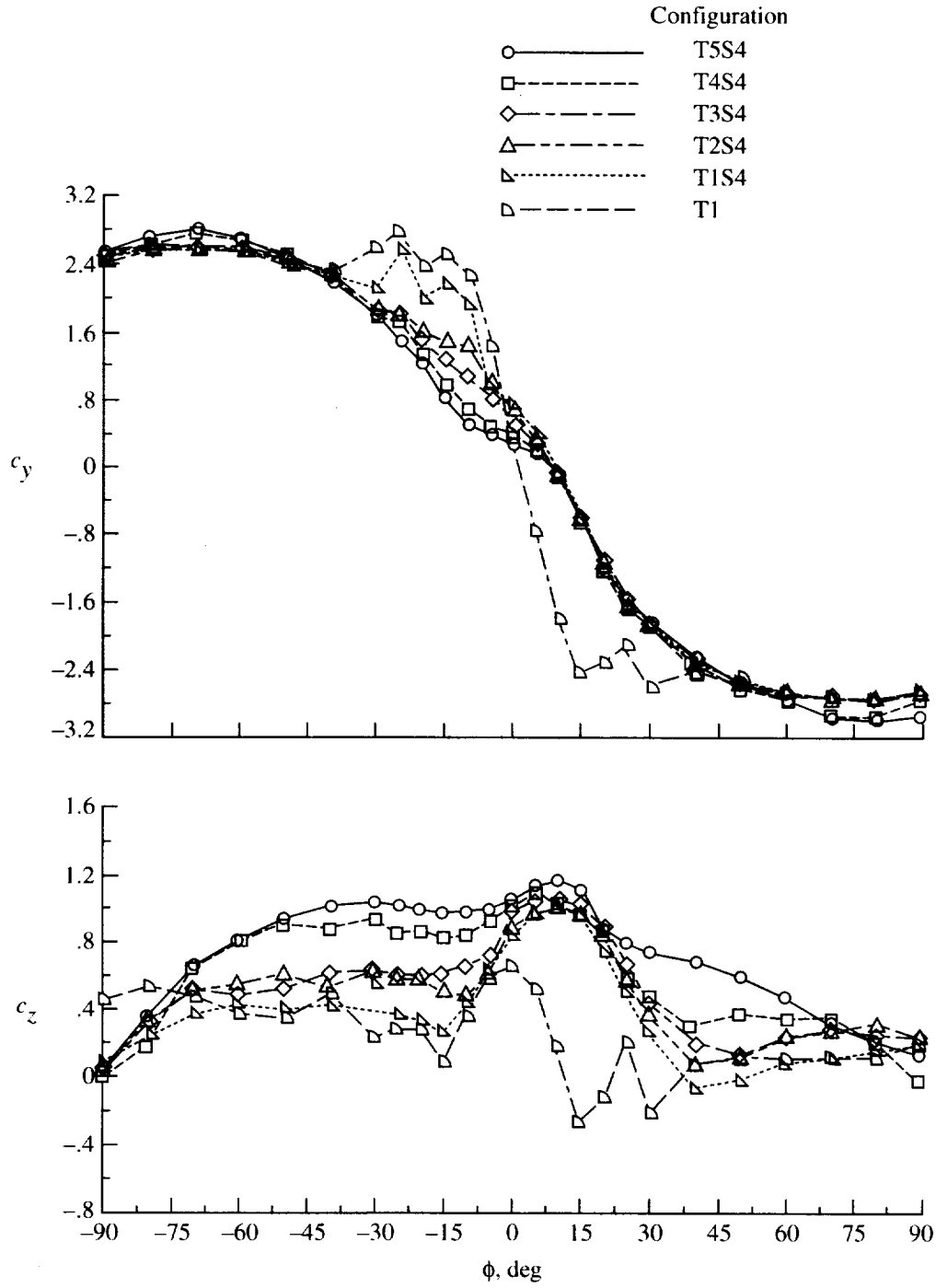

Figure 16. Effect of venting configuration and strakes on trapezoidal tail boom normal and side force coefficients for q_∞ = 20 and 25 psf.

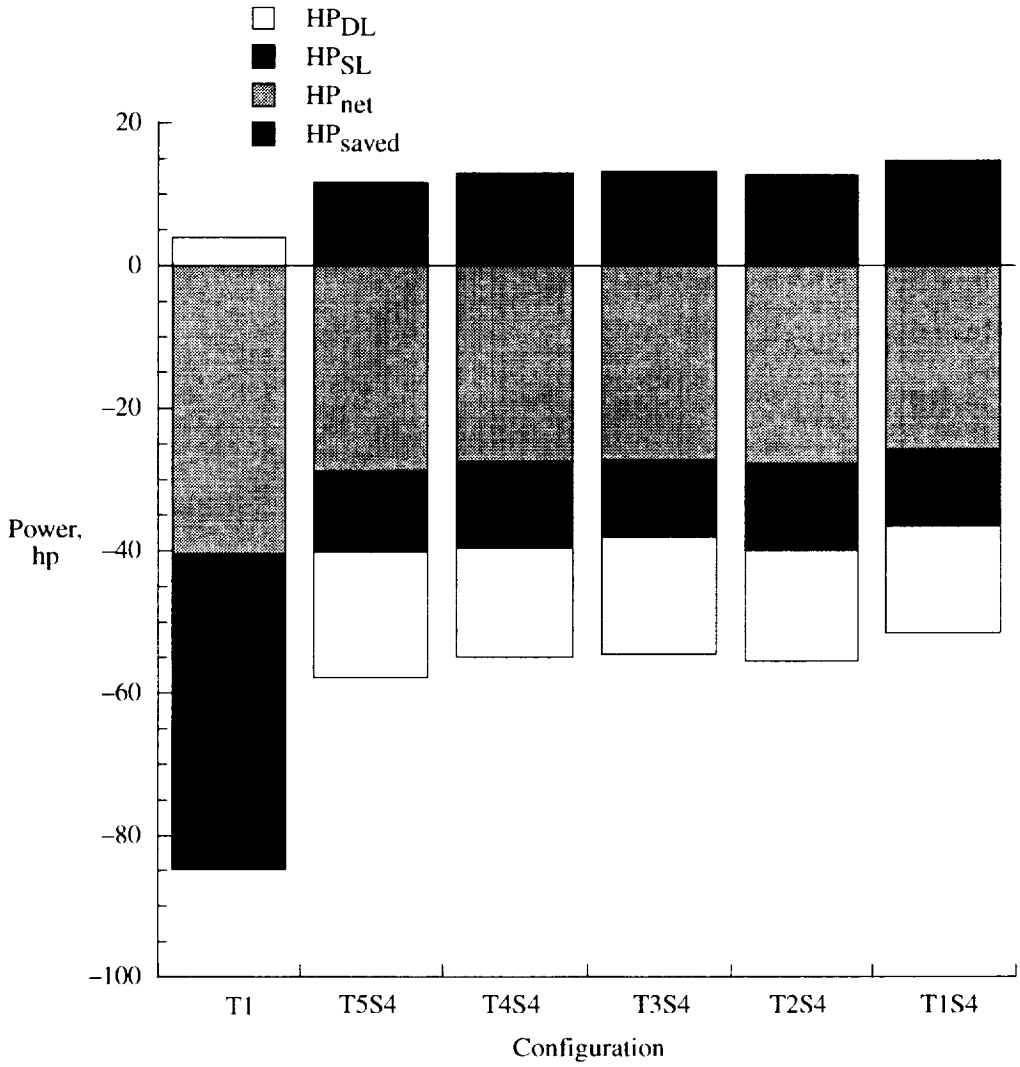

Figure 17. Calculated power required of helicopter with various tail boom configurations, trapezoidal cross section, boom strakes.

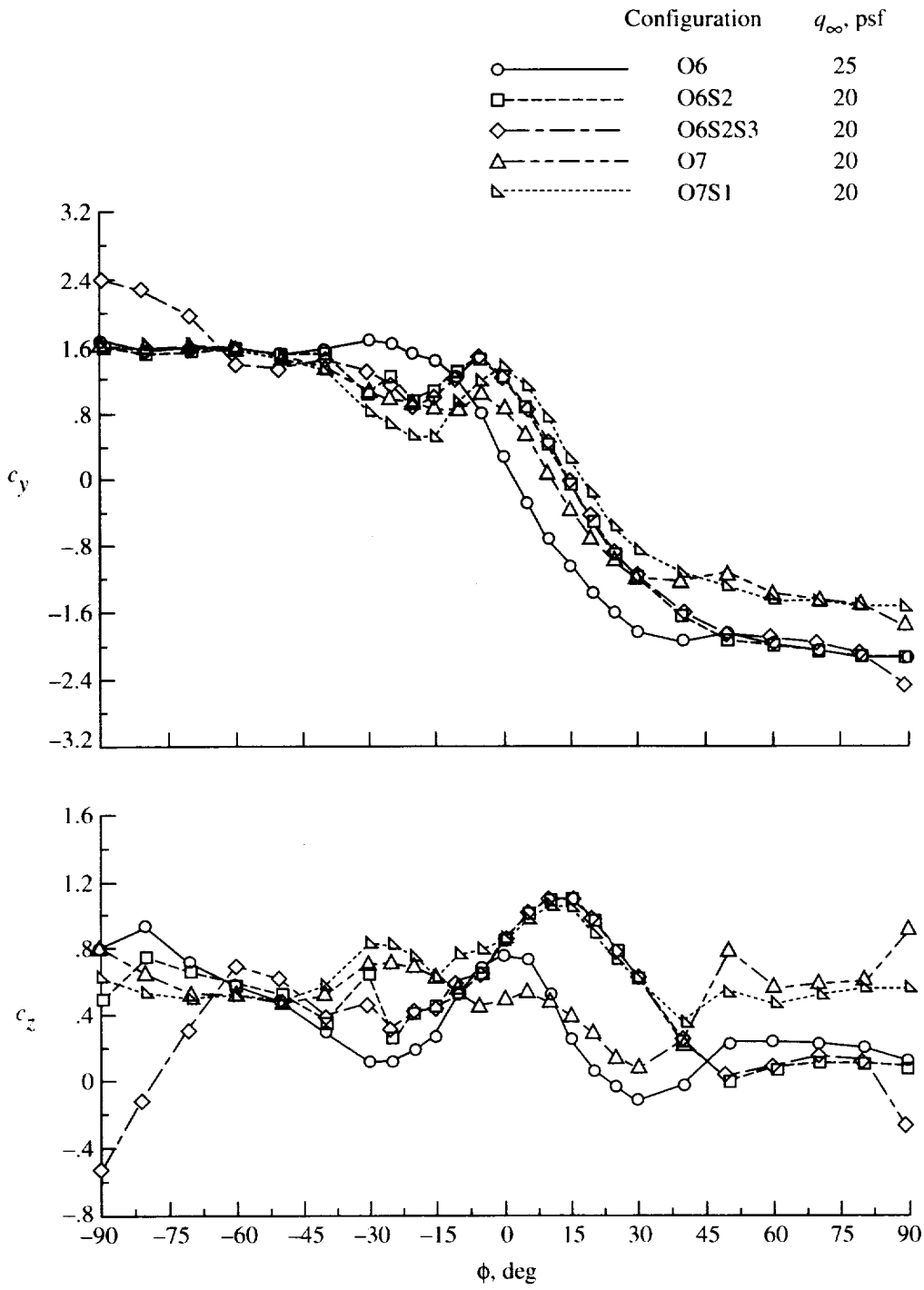

(a) q_∞ = 20 and 25 psf.

Figure 18. Effect of venting configuration and strakes on oval tail boom normal and side force coefficients for asymmetric configurations.

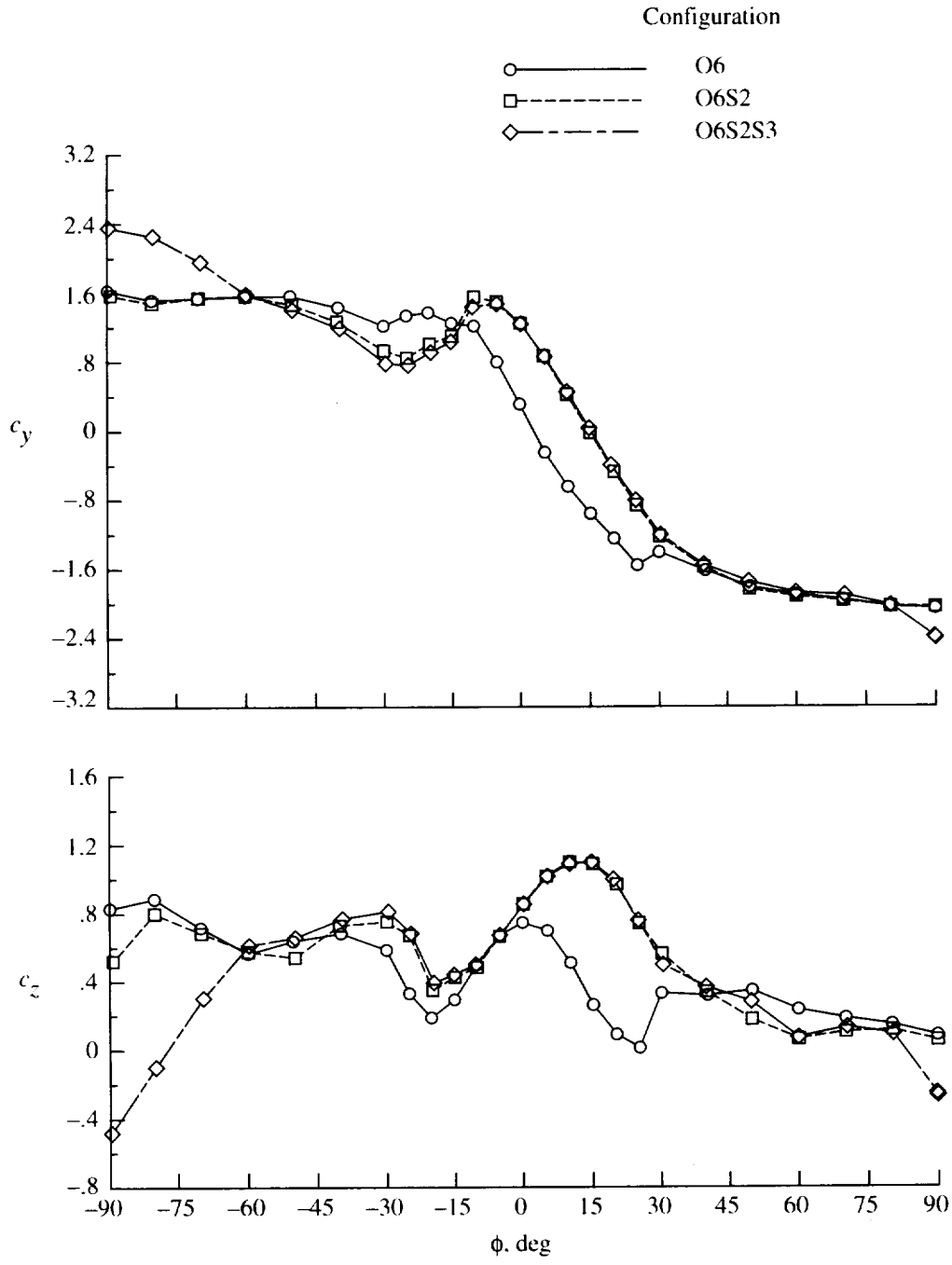

(b) q_∞ = 10 psf.

Figure 18. Concluded.

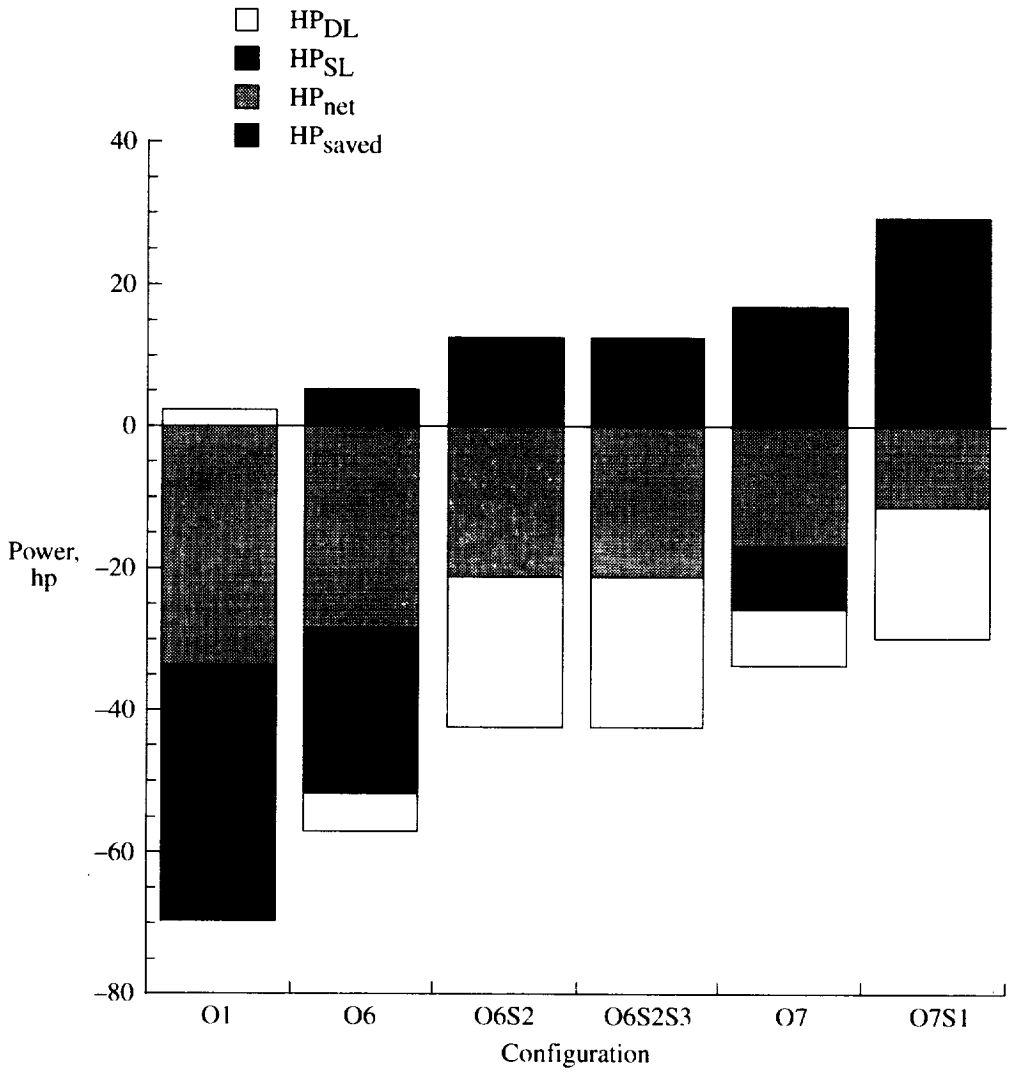

Figure 19. Calculated power required of helicopter with various tail boom configurations, oval cross section, asymmetric venting, boom strakes.

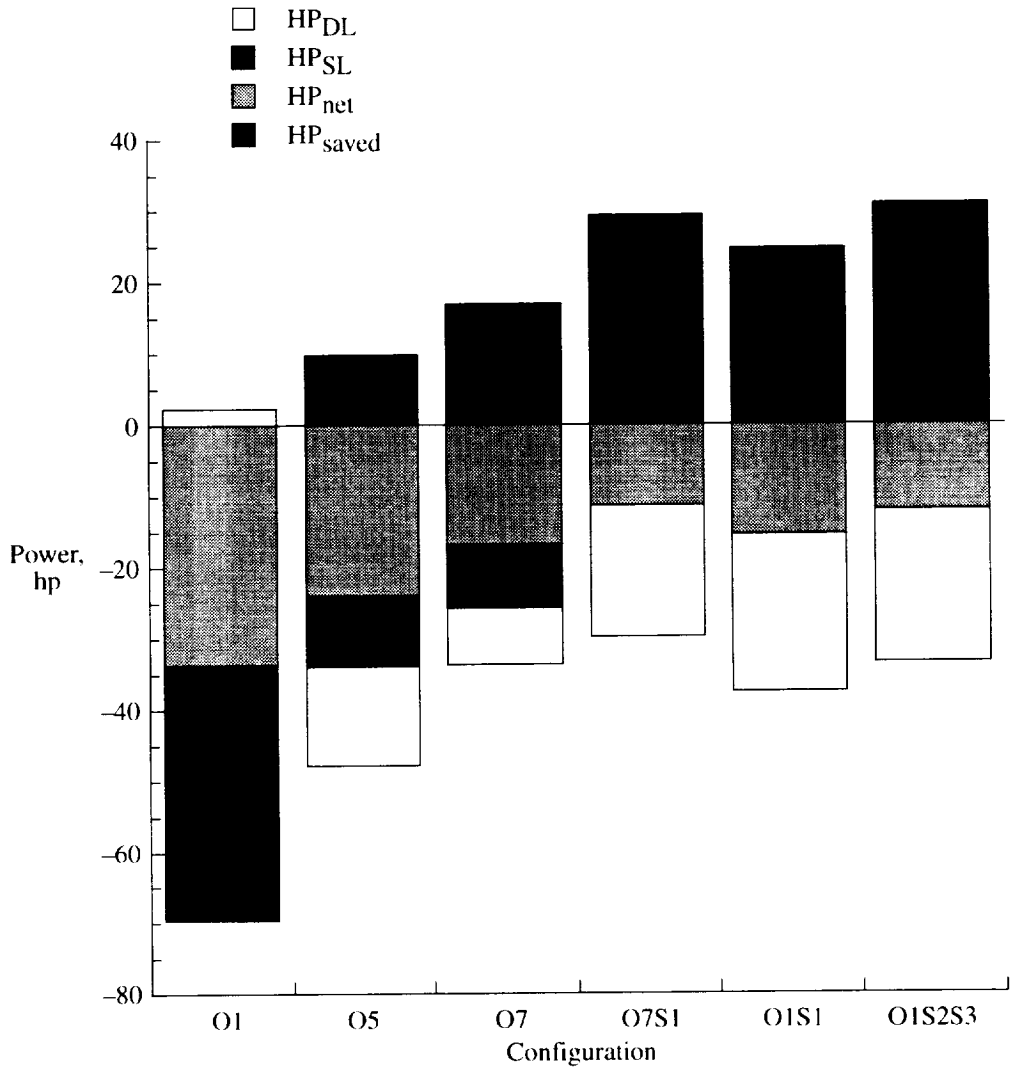

Figure 20. Calculated power required of helicopter with various tail boom configurations, oval cross-section summary.

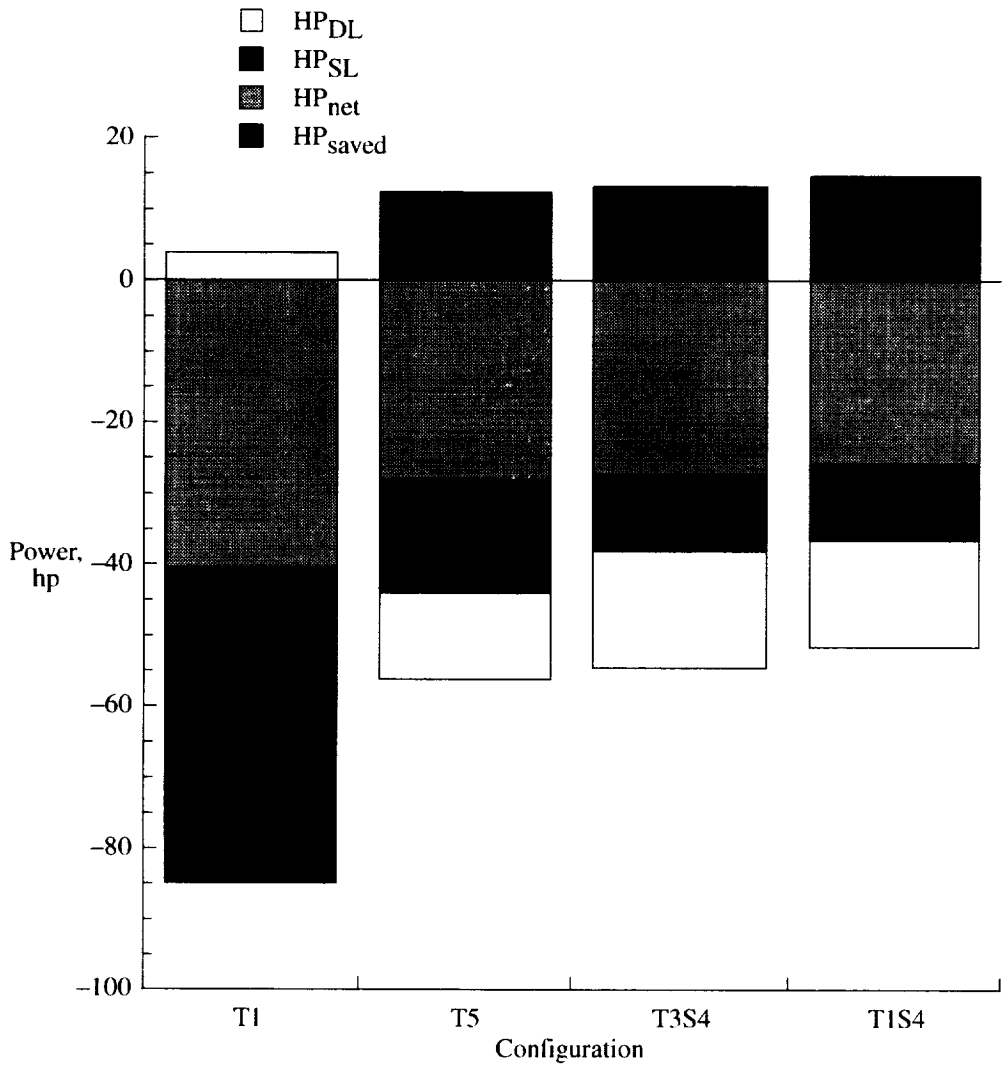

Figure 21. Calculated power required of helicopter with various tail boom configurations, trapezoidal cross-section summary.

REPORT DOCUMENTATION PAGE

Form Approved
OMB No. 0704-0188

1. AGENCY USE ONLY *(Leave blank)*	2. REPORT DATE	3. REPORT TYPE AND DATES COVERED
	June 2000	Technical Publication

4. TITLE AND SUBTITLE
Exploratory Investigation of Aerodynamic Characteristics of Helicopter Tail Boom Cross-Section Models With Passive Venting

5. FUNDING NUMBERS
WU 581-10-11-01
PR A5226

6. AUTHOR(S)
Daniel W. Banks and Henry L. Kelley

7. PERFORMING ORGANIZATION NAME(S) AND ADDRESS(ES)
NASA Langley Research Center
Hampton, VA 23681-2199

U.S. Army Aviation and Missile Command
Aeroflightdynamics Directorate
Joint Research Program Office
NASA Langley Research Center
Hampton, VA 23681-2199

8. PERFORMING ORGANIZATION REPORT NUMBER
L-17770

9. SPONSORING/MONITORING AGENCY NAME(S) AND ADDRESS(ES)
National Aeronautics and Space Administration
Washington, DC 20546-0001
and
U.S. Army Aviation and Missile Command
Moffett Field, CA 94035-1000

10. SPONSORING/MONITORING AGENCY REPORT NUMBER
NASA/TP-2000-210083
AMCOM-AFDD/TR-00-A-007

11. SUPPLEMENTARY NOTES
Banks: Dryden Flight Research Center, Edwards, CA; Kelley: AMCOM, Aeroflightdynamics Directorate, JRPO, Langley Research Center, Hampton, VA.

12a. DISTRIBUTION/AVAILABILITY STATEMENT
Unclassified–Unlimited
Subject Category 02 Distribution: Standard
Availability: NASA CASI (301) 621-0390

12b. DISTRIBUTION CODE

13. ABSTRACT ***(Maximum 200 words)***
Two large-scale, two-dimensional helicopter tail boom models were used to determine the effects of passive venting on boom down loads and side forces in hovering crosswind conditions. The models were oval shaped and trapezoidal shaped. Completely porous and solid configurations, partial venting in various symmetric and asymmetric configurations, and strakes were tested. Calculations were made to evaluate the trends of venting and strakes on power required when applied to a UH-60 class helicopter. Compared with the UH-60 baseline, passive venting reduced side force but increased down load at flow conditions representing right sideward flight. Selective asymmetric venting resulted in side force benefits close to the fully porous case. Calculated trends on the effects of venting on power required indicated that the high asymmetric oval configuration was the most effective venting configuration for side force reduction, and the high asymmetric with a single strake was the most effective for overall power reduction. Also, curves of side force versus flow angle were noticeable smoother for the vented configurations compared with the solid baseline configuration; this indicated a potential for smoother flight in low-speed crosswind conditions.

14. SUBJECT TERMS	15. NUMBER OF PAGES
Strakes; Porous surface; Tail boom	53
	16. PRICE CODE: A04

17. SECURITY CLASSIFICATION OF REPORT	18. SECURITY CLASSIFICATION OF THIS PAGE	19. SECURITY CLASSIFICATION OF ABSTRACT	20. LIMITATION OF ABSTRACT
Unclassified	Unclassified	Unclassified	UL